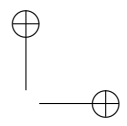
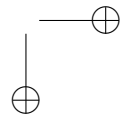
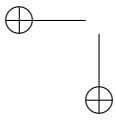
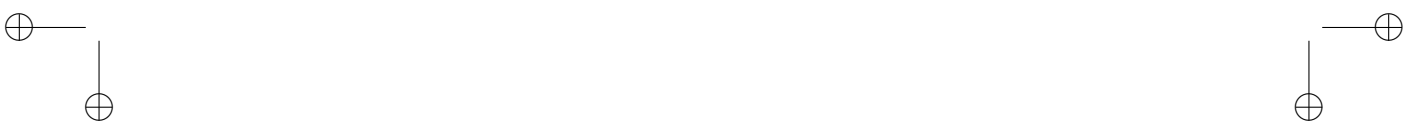


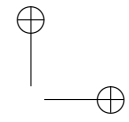
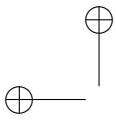
“PhDthesis\_Droghini” — 2018/11/17 — 19:52 — page i — #1



i







UNIVERSITÀ POLITECNICA DELLE MARCHE  
SCUOLA DI DOTTORATO DI RICERCA IN SCIENZE DELL’INGEGNERIA  
CURRICULUM IN INGEGNERIA ELETTRONICA, ELETROTECNICA E DELLE  
TELECOMUNICAZIONI

---

# Ambient Intelligence: Computational Audio Processing For Human Fall Detection

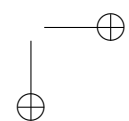
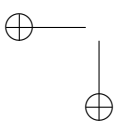
Ph.D. Dissertation of:  
**Diego Droghini**

Advisor:  
**Prof. Francesco Piazza**

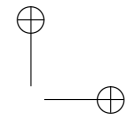
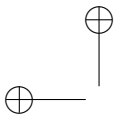
Coadvisor:  
**Prof. Roberto Bedini**

Curriculum Supervisor:  
**Prof. Francesco Piazza**

XVII edition - new series







UNIVERSITÀ POLITECNICA DELLE MARCHE  
SCUOLA DI DOTTORATO DI RICERCA IN SCIENZE DELL'INGEGNERIA  
CURRICULUM IN INGEGNERIA ELETTRONICA, ELETROTECNICA E DELLE  
TELECOMUNICAZIONI

---

# Ambient Intelligence: Computational Audio Processing For Human Fall Detection

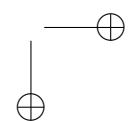
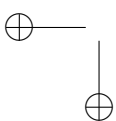
Ph.D. Dissertation of:  
**Diego Droghini**

Advisor:  
**Prof. Francesco Piazza**

Coadvisor:  
**Prof. Roberto Bedini**

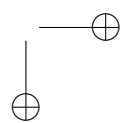
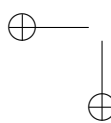
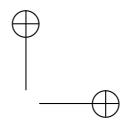
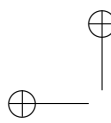
Curriculum Supervisor:  
**Prof. Francesco Piazza**

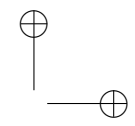
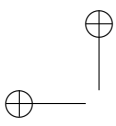
XVII edition - new series



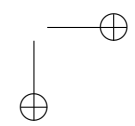
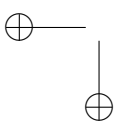
---

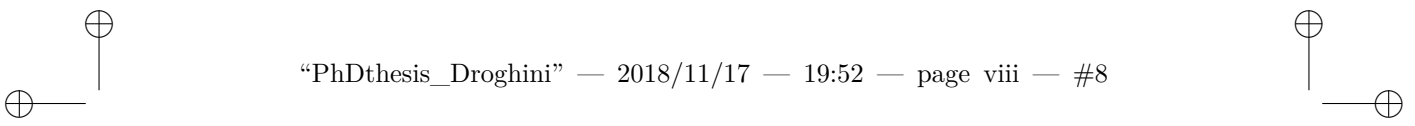
UNIVERSITÀ POLITECNICA DELLE MARCHE  
SCUOLA DI DOTTORATO DI RICERCA IN SCIENZE DELL’INGEGNERIA  
FACOLTÀ DI INGEGNERIA  
Via Brecce Bianche – 60131 Ancona (AN), Italy





*alla mia famiglia*





“PhDthesis\_Droghini” — 2018/11/17 — 19:52 — page viii — #8

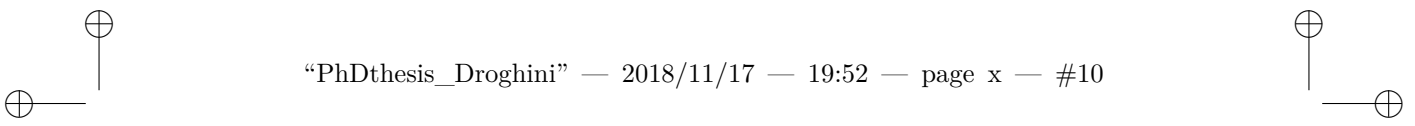


# Abstract

Lorem ipsum dolor sit amet, consectetuer adipiscing elit. Ut purus elit, vestibulum ut, placerat ac, adipiscing vitae, felis. Curabitur dictum gravida mauris. Nam arcu libero, nonummy eget, consectetuer id, vulputate a, magna. Donec vehicula augue eu neque. Pellentesque habitant morbi tristique senectus et netus et malesuada fames ac turpis egestas. Mauris ut leo. Cras viverra metus rhoncus sem. Nulla et lectus vestibulum urna fringilla ultrices. Phasellus eu tellus sit amet tortor gravida placerat. Integer sapien est, iaculis in, pretium quis, viverra ac, nunc. Praesent eget sem vel leo ultrices bibendum. Aenean faucibus. Morbi dolor nulla, malesuada eu, pulvinar at, mollis ac, nulla. Curabitur auctor semper nulla. Donec varius orci eget risus. Duis nibh mi, congue eu, accumsan eleifend, sagittis quis, diam. Duis eget orci sit amet orci dignissim rutrum.

Nam dui ligula, fringilla a, euismod sodales, sollicitudin vel, wisi. Morbi auctor lorem non justo. Nam lacus libero, pretium at, lobortis vitae, ultricies et, tellus. Donec aliquet, tortor sed accumsan bibendum, erat ligula aliquet magna, vitae ornare odio metus a mi. Morbi ac orci et nisl hendrerit mollis. Suspendisse ut massa. Cras nec ante. Pellentesque a nulla. Cum sociis natoque penatibus et magnis dis parturient montes, nascetur ridiculus mus. Aliquam tincidunt urna. Nulla ullamcorper vestibulum turpis. Pellentesque cursus luctus mauris.

Nulla malesuada porttitor diam. Donec felis erat, congue non, volutpat at, tincidunt tristique, libero. Vivamus viverra fermentum felis. Donec nonummy pellentesque ante. Phasellus adipiscing semper elit. Proin fermentum massa ac quam. Sed diam turpis, molestie vitae, placerat a, molestie nec, leo. Maecenas lacinia. Nam ipsum ligula, eleifend at, accumsan nec, suscipit a, ipsum. Morbi blandit ligula feugiat magna. Nunc eleifend consequat lorem. Sed lacinia nulla vitae enim. Pellentesque tincidunt purus vel magna. Integer non enim. Praesent euismod nunc eu purus. Donec bibendum quam in tellus. Nullam cursus pulvinar lectus. Donec et mi. Nam vulputate metus eu enim. Vestibulum pellentesque felis eu massa.



“PhDthesis\_Droghini” — 2018/11/17 — 19:52 — page x — #10



# Contents

<b>1</b>	<b>Introduction</b>	<b>1</b>
1.1	Fall Detection Systems . . . . .	1
1.2	State-Of-The-Art . . . . .	3
1.2.1	Case studies . . . . .	5
<b>2</b>	<b>Background</b>	<b>7</b>
2.1	Support Vector Machines . . . . .	7
2.1.1	One-Class Support Vector Machines . . . . .	10
2.2	Gaussian Mixture Model . . . . .	11
2.3	K-Nearest Neighbor . . . . .	12
2.4	The Artificial Deep Neural Networks . . . . .	12
2.4.1	The Human Nervous System . . . . .	12
2.4.2	Stochastic gradient descent (SGD) . . . . .	21
2.4.3	Autoencoder . . . . .	23
<b>3</b>	<b>Dataset</b>	<b>25</b>
3.1	The floor acoustic sensor . . . . .	25
3.2	The fall events dataset: A3Fall . . . . .	26
3.2.1	The recording setup . . . . .	26
3.2.2	Description . . . . .	27
3.2.3	Signal analysis . . . . .	30
<b>4</b>	<b>Supervised Approach</b>	<b>35</b>
4.1	Support-Vector Machine based algorithm for evens fall classification . . . . .	35
4.1.1	Porposed approach . . . . .	35
4.1.2	Dataset . . . . .	37
4.1.3	Experimental setup . . . . .	39
4.1.4	Results . . . . .	40
4.1.5	Remarks . . . . .	42
4.2	Binary SVM based classifier for human fall detection . . . . .	43
4.2.1	Proposed approach . . . . .	44
4.2.2	Dataset . . . . .	44
4.2.3	Experiments . . . . .	45
4.2.4	Results . . . . .	46

*Contents*

4.2.5    Remarks . . . . .	47
<b>5 Unsupervised Approach</b>	<b>57</b>
5.1    Novelty detection algorithm for human fall detection based on One-Class Support Vector Machine . . . . .	57
5.1.1    Dataset . . . . .	58
5.1.2    Experimental setup . . . . .	58
5.1.3    Results . . . . .	61
5.2    End-To-End Unsupervised Approach employing Convolutional Neural Network Autoencoders for Human Fall Detection . . . . .	62
5.3    Proposed Approach . . . . .	64
5.4    Experiments . . . . .	65
5.4.1    Dataset . . . . .	65
5.4.2    Experimental Setup . . . . .	66
5.4.3    Results . . . . .	67
5.4.4    Remarks . . . . .	68
<b>6 Semi-Unsupervised Approach</b>	<b>71</b>
6.1    A Combined One-Class SVM and Template Matching Approach for User-Aided Human Fall Detection . . . . .	71
6.1.1    Proposed approach . . . . .	73
6.1.2    Dataset . . . . .	74
6.2    Few-shot Siamese Neural Networks employing Audio features for Human-Fall Detection . . . . .	75
6.3    Audio Metric Learning by using Siamese Autoencoders for One-Shot Human Fall Detection . . . . .	75
<b>7 Other contributions</b>	<b>77</b>
<b>List of Publications</b>	<b>79</b>

## List of Figures

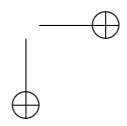
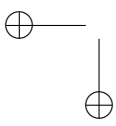
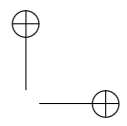
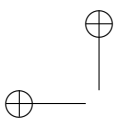
2.1	A hyperplane separating two classes with the maximum margin. The red highlighted points are the support vectors. . . . .	8
2.2	The human brain. . . . .	12
2.3	The neuron model. . . . .	13
2.4	The Artificial Neural Network. . . . .	13
2.5	The artificial neuron model. . . . .	15
2.6	The threshold non-linear function. . . . .	16
2.7	The sigmoid non-linear function. . . . .	16
2.8	The <i>tanh</i> non-linear function. . . . .	17
2.9	The <i>ReLU</i> non-linear function. . . . .	17
2.10	The <i>softmax</i> layer in a neural network classifier. . . . .	18
2.11	The Multilayer Feedforward Network. . . . .	19
2.12	The Convolutional Neural Network. . . . .	19
2.13	The convolution operation. . . . .	20
2.14	The max-pooling layer. . . . .	20
2.15	The different types of Autoencoders. . . . .	23
3.1	The floor acoustic sensor: conceptual scheme. 1 - The outer container. 2 - The inner container. 3 - The microphone slot. 4 - The membrane touching the floor. . . . .	26
3.2	A picture of the floor acoustic sensor used during the recordings.	27
3.3	Objects employed for creating the fall events dataset. . . . .	29
3.4	Falls of the “Rescue Randy” doll from upright position (a) and from the chair (b). . . . .	30
3.5	The recording room: the letters A, B, C and D indicate the positions of fall events. . . . .	31
3.6	Frequency content of the same fall event (file “rndy_d2st_bar_0.wav”) acquired with the FAS (a) and with the aerial microphone (b).	32
3.7	Average value of the mel channels. . . . .	33
3.8	Average value of the SNR for each mel channel. . . . .	33
4.1	The MFCC feature extraction pipeline. . . . .	36
4.2	Block scheme for extracting a gaussian mean supervector from MFCCs and a trained UBM. . . . .	37
4.3	Block scheme for training the UBM and SVM models. . . . .	38

*List of Figures*

4.4	Block-scheme of the fall classification phase. . . . .	38
4.5	Fall classification performance in matched condition with clean (a) and noisy signals (b). . . . .	50
4.6	Fall classification performance in mismatched condition. . . . .	51
4.7	Fall classification performance in multicondition. . . . .	52
4.8	Fall classification performance in matched condition with the dataset comprising everyday noises. . . . .	53
4.9	Fall classification performance in mismatched condition with the dataset comprising everyday noises. . . . .	54
4.10	Fall classification performance in multicondition with the dataset comprising everyday noises. . . . .	55
5.1	Results in <i>clean</i> conditions for the three test cases. “Set 1” comprises human falls, human activities and music. “Set 2” comprises human falls and object falls. “Set 3” comprises human falls, object falls, human activities, and music. . . . .	62
5.2	Results in <i>noisy</i> conditions for the three test cases. “Set 1” comprises human falls, human activities and music. “Set 2” comprises human falls and object falls. “Set 3” comprises human falls, object falls, human activities, and music. . . . .	63
5.3	The proposed approach scheme. . . . .	64
5.4	Results in <i>clean</i> and <i>noisy</i> conditions for the three test cases. .	68
6.1	Time domain (on the left) and frequency domain (on the right) representation of a normal human activity signal (a-b), human fall signal (c-d), and book fall signal (e-f). . . . .	72
6.2	The block scheme of the proposed approach. . . . .	74

# List of Tables

3.1	Composition of the A3Fall-v2.0 dataset.	28
4.1	Data related to R0 room used in this work.	39
4.2	Aerial microphone confusion matrix related to the STD configuration in clean condition. The average precision is 91.48%, the average recall 91.23%, and the average F <sub>1</sub> -Measure 91.04%.	41
4.3	FAS confusion matrix related to the NPRELP configuration in clean condition. The average precision is 98.13%, the average recall 98.05%, and the average F <sub>1</sub> -Measure 98.06%.	42
4.4	Data related to R0 room used in this work.	45
4.5	Fall classification performance in matched condition with the dataset excluding everyday noises.	47
4.6	Fall classification performance in mismatched condition (a) and multicondition (b) with the dataset excluding everyday noises. F <sub>1</sub> denotes the F <sub>1</sub> -Measure.	48
5.1	Composition of the dataset.	58
5.2	Composition of the training-set.	59
5.3	Composition of “Set 1”.	59
5.4	Composition of “Set 2”.	60
5.5	Composition of “Set 3”.	60
5.6	Hyperparameters of the algorithm and search space explored in the validation phase.	61
5.7	Composition of the dataset.	66
5.8	Hyper-parameters optimized in the random-search phase, and their range.	67
5.9	Best hyper-parameters find in random-search phase for <i>clean</i> and <i>noisy</i> condition	67



# Chapter 1

## Introduction

Ambient intelligence + computation audio processing + obiettivi, controbuti,  
Outline

The decreasing birth rate [1] and the contemporary increase of the life expectancy at birth [2] in the majority of industrialized countries have been generating new challenges in the assistance of the elderly. The scientific community, companies and governments are trying to face them by investing in the development of efficient healthcare systems and solutions. The direction taken goes towards the development of smart home capable of taking care of the inhabitants by supporting and monitoring them in their daily actions [3, 4]. Since falls are one of the main cause of death for the elderly [5], several efforts have been devoted to the development of algorithms for automatically detecting these events.

### 1.1 Fall Detection Systems

The continuous and unprecedented growth rate of the elderly world population is one of the primary aspects of concern for society and governments. Nowadays about 8.5% of people in the world are more than 65 years old [6, 2]. Although the average life of the world population is getting longer, elderly people may not necessarily live a healthier life. It is enough to say that 37.5 million falls require medical interventions and more than 600 thousand are cause of death every year worldwide. In particular, the population segment most affected by this problem is composed of elderly over 65 years that, with the growing mobility of the population, are more frequently left alone in their homes without aid in the case of need. Moreover, since falls are the leading cause of death and hospitalizations for older adults, this phenomenon leads to a substantial increase in the cost of healthcare [7, 5]. It is not surprising, thus, that the research community is encouraged, even by governments, to find reliable and performing solutions to minimize the damage caused by the human falls problem. This is also confirmed by the presence in the literature of several reviews dedicated to this specific topic [5, 8, 9, 10, 11, 12]. In fact, in the past few years, a variety

## Chapter 1 Introduction

of systems have been presented. One way to divide the methodologies for approaching the falls detection problem is based on the placement of the sensing devices [5]. The main categories are wearable, vision and environmental, with each category presenting their own advantages and disadvantages. Wearable systems do not suffer from ambient condition, but people may forget to wear them and they are not operational during the charging time, thus, some people may consider them annoying. Furthermore, a device must be installed on each person to be monitored. An environmental sensor may be used to avoid this kind of problems, but with other limitations. Vision systems, although they are actually environmental sensors, deserve a dedicated category because of many systems proposed in the literature based on this type of sensors [5]. This category includes several types of sensors like, e.g., cameras for which the major limitations are field-of-view constraints, lighting condition, positioning of multiple cameras and lack of privacy. The ambient category includes several types of sensors. For example, radar doppler based systems used in [13] raise fewer privacy concerns, but they suffer from reflection and blind spots. In particular, for a data-driven system, another aspect that should not be underestimated is the need for a re-training when changing the environment to be monitored or even just some of its components such as the arrangement of furniture as happens in [14]. All this implies that there is no optimal choice, which is instead, a compromise that depends on the type of environment that is monitored as well as on personal sensitivity of the subjects under monitoring. Going into more detail, another significant distinction between falls detection systems can be made based on the type and amount of data used for the algorithm development [8]. In fact, the problem can be approached either as supervised or unsupervised based on the availability of data in the hands of the researchers as well as their goals. Most state-of-the-art works tackle the problem under fully supervised conditions assuming they have enough data for falls. Almost all of these falls are simulated with professional mannequins [15, 16] or by people with adequate protections [17, 18] that however may not correctly emulate an actual fall. Although this approach leads to more accurate results, there is no guarantee that it will generalize well in real situations. Other researchers opt for approaches based on outlier/anomaly detection [19, 20, 21] because of the plentiful availability of data that can represent normal activity. However, it is challenging to define what “normal activities” are for such approaches, and the risk is to raise several false alarms. Perhaps the situation that most closely approximates reality is a hybrid between the previous ones, in which a large amount of data representing the normality are easily available, with just a few samples of real human fall (*RHF*) and eventually some related synthetic or simulated data. In these situations, supervised approaches that suffer from strong data imbalance have to apply subsampling [22] or weighting [8] tech-

## 1.2 State-Of-The-Art

niques to mitigate this effect. Thus, the need to find an effective way to exploit the few available falls data is evident.

### 1.2 State-Of-The-Art

Review dei sistemi per la fall detection basati sui vari tipi di sensori accelerometers, vision, ambient. Per gli ambient paricolare enfasi sugli approcci basati su aduio.

As aforementioned, fall detection approaches can be divided based on their sensing technology, in particular if they employ wearable or ambient sensors. Regarding the first ones, the most common choice is to employ accelerometers. The algorithms proposed in [23] and [24] detect a fall by verifying if the acceleration signals exceed a certain threshold. In contrast, in [25] the authors implemented several machine learning techniques and studied their classification performance. For the experiments, a fall events dataset has been developed using six sensor units with three-axis accelerometers and worn by 14 persons who simulated falls from different angles. The best performing classifier resulted the  $k$ -Nearest Neighbour classifier. [26] employed radio tags worn on the user’s chest, waist, and ankles, and an optional three-axial accelerometer worn on the chest. The algorithms performs a basic activity recognition, distinguishing from walking, standing, sitting, sitting on the ground, lying down, the process of sitting or lying down, the process of standing up, and falling. The actual fall is detected combining the results of two classifiers, an SVM and a decision tree, and hand-crafted rules. The authors performed the experiments on a laboratory scenario and reported accuracies of 100% combining radio tags and the accelerometer.

Differently from wearable sensors, the physical quantities captured by ambient sensors are more heterogeneous. Generally, fall detectors are based on vibration, video or acoustic sensors, sometimes in combination with presence detectors. In [27] the fall detector is based on a floor vibration sensor and the algorithm detects a fall when the vibration pattern matches the one of a human fall. The authors do not give further details on the algorithm and report 100% sensitivity and specificity on tests conducted on a dummy falls dataset. Yazar and colleagues [28] employ both passive infrared (PIR) sensors and floor vibration sensors. PIRs are employed to reduce false alarms, i.e., by detecting if a person is present in the region of interest. Single-tree complex wavelet transform features are extracted from the vibration signal and classified as fall or non-fall. In their dataset, the non-fall classes are represented by human (walking or running and sitting) or non-human activities (door slamming and a book falling). Three different classifiers have been compared: Euclidean distance, Mahalanobis distance and SVM, with the latter resulting in the most

## Chapter 1 Introduction

performing one, since it is able to classify human falls without errors regardless the employment of PIR sensors.

Regarding approaches based on audio signals, a common solution is to install several microphones in the building, usually on the ceiling or near the walls. Indeed, also single-microphone approaches exist but they are much less robust to environmental noise, thus resulting in poor performance. For example, in [29], the authors employ a single far field microphone and they model audio segments by means of perceptual linear predictive (PLP) coefficients and GMM supervectors. An SVM with a kernel based on the Kullback-Leibler divergence, then, classifies the segment as being a fall or noise. For this purpose, nine classes of noise have been considered. In the experiments, the algorithm achieves an F<sub>1</sub>-Measure of 67% in the classification task, and an accuracy equal to 64% in the detection task.

The difficulty in using a single microphone drove the scientific community to employ multi-channel algorithms. In [19] the authors present an unsupervised algorithm based on two microphones. The algorithm comprises a source separation and localization block to reduce the impact of background noise. Then, a one class Support Vector Machine is trained on MFCCs of non-fall events only. The SVM is then applied to distinguish normal sound events (i.e., sounds originating from normal activities) from abnormal ones (i.e., falls sounds). The authors validated the algorithm using simulated falls of persons only in presence of a television that produced the interfering sound. The results in terms of Area Under Curve are 0.9928 without interference and 0.9738 with 75% interference. The work by Li and colleagues [17] employs a circular microphone array to firstly determine the position of the sound source, and then to enhance the signal by applying a beamformer. The height of the sound source is used as first filter to discriminate falls from non falls. If the sound originates from a source positioned on the ground, MFCC features are extracted and a k-Nearest Neighbour classifier is employed to detect persons’ falls. The algorithm has been tested on a dataset composed of 120 simulated fall sounds and 120 non-fall sounds recorded in different acoustic conditions. In presence of background noise and TV interference, the resulting AUC was equal to 0.989 (accuracy 95%) on clean conditions and 0.932 at 10 dB SNR (accuracy 89%).

An approach to improve the performance of fall detection systems is to combine the information coming from different sensors. The approach proposed by Zigel *et al.* [16] is based on a combination of sound and vibration sensors attached to the floor with a adhesive tape. The algorithm employs energy features extracted from the vibration signal to detect the fall event. Then, the event is classified as fall or non-fall with naive Bayes classifier employing features from both the vibration and sound signals. The experiments were conducted on a dataset containing falls of the “Rescue Randy” human mimicking doll and four

## 1.2 State-Of-The-Art

objects, and the resulting sensitivity and specificity were respectively 97.5% and 98.6%. [30] fuse the information coming from a Doppler sensor and motion sensors and classify falls with an SVM. The authors report an AUC equal to 0.98 with Doppler sensor only, and a further reduction of false alarms by 63% employing motion sensors information. Motion, sound and video signals are employed in [31]. Signals are captured both from environment sensors and from body sensors. A fall is detected by analysing sounds and motion information, while visual and motion behaviour indicates the severity of the fall. The work by Toreyin and colleagues [32] combines PIRs, microphones and vibration sensors. Signals are processed to extract features in the wavelet domain and an HMM classifier is then employed to detect falls. The authors showed the using PIR signals 100% accuracy can be obtained.

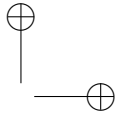
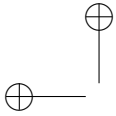
### 1.2.1 Case studies

Generally speaking, the “analytical methods” distinguish between fall and non-fall events by applying a threshold directly on the acquired signals or on the features sequences extracted from them [33]. These methods are generally built exploiting some a-priori knowledge to operate in a specific scenario and needs manual tuning of the hyperparameters of the algorithm. For these reasons, the “analytical methods” can hardly perform when the operating conditions and the subjects are variable. In “machine learning” methods, the algorithm learn from the data how to discriminate falls from non-falls [33]. Between them can be distinguished “supervised” and “unsupervised” approaches. The first require a labelled dataset for training the classifier, while the latter build a normality model considering only the non-fall events. Regardless of the used approach, machine learning tasks require that the inputs are mathematically and computationally convenient to process, so researchers have traditionally relied on a two-stage strategy: some features are extracted from the raw signals of dataset and are then used as input for the successive tasks. The choice and design of the appropriate features requires considerable expertise about the problem and constitutes a significant engineering effort.

In this work, different application of computational audio processing based on machine learning techniques for ambient intelligence are analyzed. Particular attention was given to the condition of knowledge for each proposed approach. In fact, the presented works start from a total knowledge of the data describing first the supervised methods dedicated to the falls detection. Because of the difficulty in recovering examples of human fall for algorithm training, this is primarily just a case study. Subsequently, methods that operate in the opposite condition are described, that is, without the a priori knowledge of signals related to the human fall. This would be the ideal condition, but that does not present

## *Chapter 1 Introduction*

very high reliability in terms of false alarms rate. Finally, the problem is dealt with from a more realistic point of view, in which only a small portion of data related to the human fall is available, while a vast knowledge of what is not human fall can be accessed.



# Chapter 2

## Background

In recent years, the IoT revolution has led to the creation of enormous amounts of data. The use of intelligent devices that can interface with cloud computing systems or perform complex calculations directly on board, in homes and cities, has allowed the affirmation of data-driven algorithms compared to other methodologies used so far. In fact, these approaches try to emulate the functioning of the human mind, enabling computers to perform tasks that are unthinkable until now. In this chapter are resumed the data-driven and machine learning algorithms used for developing the proposed methodologies for fall classification systems.

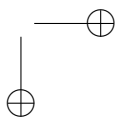
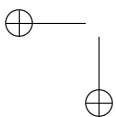
### 2.1 Support Vector Machines

Support Vector Machines (SVM) [34] are one of the most popular classification algorithms and are well known for their strong theoretical foundations, generalization performance and ability to handle high dimensional data. This section presents an overview of support vector machine, starting with linear SVMs, followed by their extension to the nonlinear case and finally the One-Class SVM for novelty detection.

**Linear Support Vector Machines** In the binary classification setting, let  $((x_1, y_1) \dots (x_n, y_n))$  be the training dataset where  $x_i \in \Re^n$  are the  $n$ -dimensional feature vectors representing the instances (i.e. observations) and  $y_i \in \{-1, +1\}$  be the labels of the instances. Support vector learning is the problem of finding a separating hyperplane that separates the positive examples (labeled +1) from the negative examples (labeled -1) with the largest margin:

$$f(\vec{w}) = \text{sign}(\vec{w}^T \cdot \vec{x} + b), \quad (2.1)$$

where a value of  $-1$  indicates one class, and a value of  $+1$  the other class. In the simpler linearly separable problem, the margin of the hyperplane is defined as the shortest distance between the positive and negative instances that are



## Chapter 2 Background

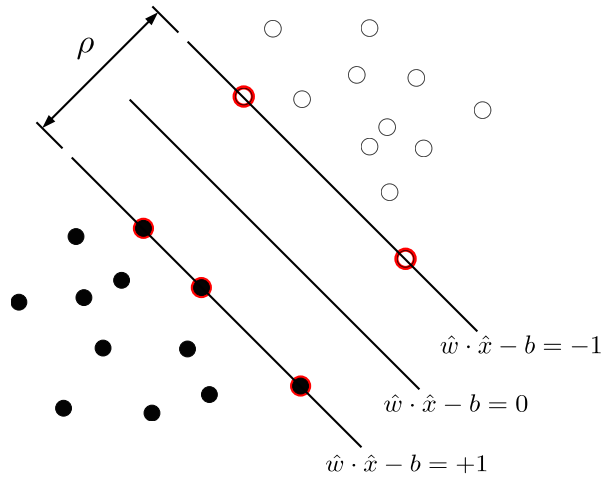


Figure 2.1: A hyperplane separating two classes with the maximum margin. The red highlighted points are the support vectors.

closest to the hyperplane. The intuition behind searching for the hyperplane with a large margin is that a hyperplane with the largest margin should be more resistant to noise than a hyperplane with a smaller margin.

Formally, suppose that all the data satisfy the constraints

$$\vec{w} \cdot \vec{x}_i + b \geq +1 \text{ for } y_i = +1, \quad (2.2)$$

$$\vec{w} \cdot \vec{x}_i + b \leq +1 \text{ for } y_i = -1, \quad (2.3)$$

where  $\vec{w}$  is the normal to the hyperplane,  $\frac{|b|}{\|\vec{w}\|}$  is the perpendicular distance from the hyperplane to the origin, and  $\|\vec{w}\|$  is the Euclidean norm of  $\vec{w}$ . These two constraints can be expressed in compact form as:

$$y_i(\vec{w} \cdot \vec{x}_i + b) \geq 1. \quad (2.4)$$

The *canonical hyperplane* is the hyperplane that separates the data and has maximal margin. The margin  $\rho$  can be computed as the distance between the two canonical hyperplanes:

$$\rho = \frac{1 - b}{\|\vec{w}\|} - \frac{-1 - b}{\|\vec{w}\|} = \frac{2}{\|\vec{w}\|} \quad (2.5)$$

Thus, we need to solve an optimisation problem, finding the hyperplane that maximises the margin and ensures the classes are separable

$$\min_{\vec{w}, b} \frac{1}{2} \|\vec{w}\|^2 \text{ subject to } y_i(\vec{w} \cdot \vec{x}_i + b) \geq 1. \quad (2.6)$$

## 2.1 Support Vector Machines

The problem can be expressed in the Lagrangian formulation:

$$\mathcal{L}(\vec{w}, b, \lambda) = \frac{1}{2} \|\vec{w}\|^2 + \sum_{i=1}^m \lambda_i (1 - y_i (\vec{w} \cdot \vec{x}_i + b)) \quad (2.7)$$

with Lagrange multipliers  $\lambda_i \geq 0$  for each constraint in 2.6. The objective is then to minimize 2.7 with respect to  $\vec{w}$  and  $b$  and simultaneously require that the derivatives of  $\mathcal{L}(\vec{w}, b, \lambda)$  with respect to all the  $\lambda$  vanish. The advantage is twofold: the training vectors only appear as a scalar product among the vectors, and the constraints are easier to manage.

With the formulation presented above, the SVM fails in some situation. In fact, there is no solution if samples can not be separated by a hyperplane. Moreover, although data are linearly separable the SVM may overfit to some outlier compromising system performance. For dealing with this type of problem, has been developed the soft margin SVM [34] which allows data points to lie within the margins. Introducing *slack variables*  $\xi_i$  into the constraints and penalize them in objective, the new problem becomes

$$\min_{\vec{w}, b, \xi} \frac{1}{2} \|\vec{w}\|^2 + C \sum_{i=1}^m \xi_i \quad (2.8)$$

subject to  $y_i (\vec{w} \cdot \vec{x}_i + b) \geq 1 - \xi_i$  and  $\xi_i \geq 0$  for  $i = 1 \dots m$ .

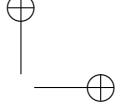
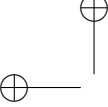
The cost coefficient  $C > 0$  is a hyper-parameter that specifies the misclassification penalty and is tuned by the user based on the classification task and dataset characteristics.

**Non-Linear Support Vector Machines** A way to solve the problem when data are not linearly separable, is to map the data on to a higher dimensional space and then to use a linear classifier in the higher dimensional space. This methods is referred to as “the kernel trick ” that exploit the fact that the training data appears as a dot product between vectors in the Lagrangian formulation to from non-linear decision boundaries. Suppose to use a transformation  $\Phi : \vec{x} \rightarrow \phi(\vec{x})$  to map every data sample into higher dimensional space, the dot product becomes  $\phi(\vec{x}_i)^T \phi(\vec{x}_j)$ . By the use of a kernel function

$$K(\vec{x}_i, \vec{x}_j) = \langle \phi(\vec{x}_i), \phi(\vec{x}_j) \rangle, \quad (2.9)$$

it is possible to compute the separating hyperplane without explicitly carrying out the mapping into feature space. The classifier become:

$$f(\vec{x}) = \text{sign} \left( \sum_i \lambda_i y_i K(\vec{x}_i, \vec{x}) + b \right) \quad (2.10)$$



## Chapter 2 Background

The most popular kernel functions are:

- Linear Kernel:

$$K(\vec{x}_i, \vec{x}_j) = \langle \vec{x}_i, \vec{x}_j \rangle \quad (2.11)$$

- Polynomial Kernel:

$$K(\vec{x}_i, \vec{x}_j) = (\langle \vec{x}_i, \vec{x}_j \rangle)^d \quad (2.12)$$

- Sigmoid Kernel:

$$K(\vec{x}_i, \vec{x}_j) = \tanh(\gamma \langle \vec{x}_i, \vec{x}_j \rangle - \theta) \quad (2.13)$$

- RBF Kernel:

$$K(\vec{x}_i, \vec{x}_j) = \exp\left(-\frac{\|\vec{x}_i - \vec{x}_j\|}{2\sigma^2}\right) \quad (2.14)$$

Up to now the SVM algorithm for binary classification has been described. This algorithm can be extended to the multi-class case using the “one vs all” technique [35].

### 2.1.1 One-Class Support Vector Machines

One-Class SVM (OCSVM) proposed by Schölkopf et al. [36] is the extension of the support vector machine to the case of unlabeled data that makes them useful for novelty detection problems. In the OCSVM, a new parameter  $\nu$  that controls the trade-off between maximizing the distance of the hyperplane from the origin and the number of data points contained by the hyperplane has been introduced. To separate the data from the origin, the following quadratic program has to be solved:

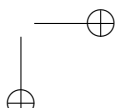
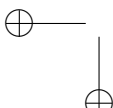
$$\min_{\vec{w}, \xi, \rho} \frac{1}{2} \|\vec{w}\|^2 + \frac{1}{\nu l} \sum_{i=1}^m \xi_i - \rho \quad (2.15)$$

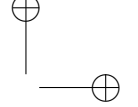
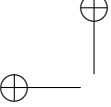
subject to  $(\vec{w} \cdot \phi(\vec{x}_i)) \geq \rho - \xi_i$  and  $\xi_i \geq 0$  for  $i = 1 \dots m$ .

In fact, One-Class SVM consists in a discriminant function that takes the value  $+1$  in a small region that captures the majority of the data points of a set and  $-1$  outside that region [37]. The discriminant function has the following expression:

$$f(\mathbf{x}) = \text{sgn} \left( \sum_i \alpha_i \cdot k(\mathbf{x}_i, \mathbf{x}) - \rho \right), \quad (2.16)$$

where  $\vec{x}_i$  denotes the  $i$ -th support vector. The position of the hyperplane, thus, defines the region that represents normal data points. For each point  $\mathbf{x}$  that lies outside this region, the function  $f(\vec{x})$  takes the value  $-1$ , whereas for point





## 2.2 Gaussian Mixture Model

inside the region, it takes the value +1. The terms  $\lambda_i$  can be found by solving the solution to the dual problem:

The terms  $\lambda_i$  can be found by solving the solution to the dual problem:

$$\min_{\lambda} \frac{1}{2} \sum_{ij} K(\vec{x}_i, \vec{x}_j) \quad (2.17)$$

$$\text{subject to } 0 \leq \lambda_i \leq \frac{1}{\nu l} \quad \text{and} \quad \sum_i \lambda_i = 1,$$

where  $\lambda_i$  is a Lagrange multiplier and  $l$  is the number of points in the training dataset. The term  $\nu \in (0, 1]$  is an hyperparameter of the algorithm that is determined on a validation set.

The offset  $\rho$  can be obtained from the Karush-Kuhn-Tucker (KKT) condition with the expression [38]:

$$\rho = \sum_j \lambda_i k(\vec{x}_j, \vec{x}_i), \quad (2.18)$$

which is satisfied for any  $\lambda_i$  that is not at the upper or lower bound.

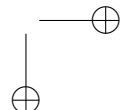
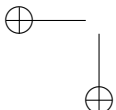
## 2.2 Gaussian Mixture Model

TODO CAMBIA/integra CON CIN <https://pdfs.semanticscholar.org/734b/07b53c23f74a3b004d7fe341ae4f>  
A Gaussian Mixture Model (GMM) is a parametric probability density function represented as a weighted sum of Gaussian component densities. Generally, GMMs are used as a parametric model of the probability distribution of some features. To estimate the parameter of GMM the algorithm Expectation-Maximization (EM) algorithm or Maximum A Posteriori (MAP) are used starting from a well-trained prior model usually named Universal Background Model (UBM). A Gaussian mixture model is a weighted sum of  $M$  component Gaussian densities as given by the equation

$$p(\vec{x}, \lambda) = \sum_{i=1}^M w_i g(\vec{x} | \vec{\mu}_i, \vec{\Sigma}_i) \quad (2.19)$$

where  $\vec{x}$  is a D-dimensional features vector,  $g(\vec{x} | \vec{\mu}_i, \vec{\Sigma}_i)$  are the components of the mixture and  $w_i$  are the weight of each component. Each component of the mixture is a D-variate Gaussian density function expressed as

$$a \quad (2.20)$$



## Chapter 2 Background

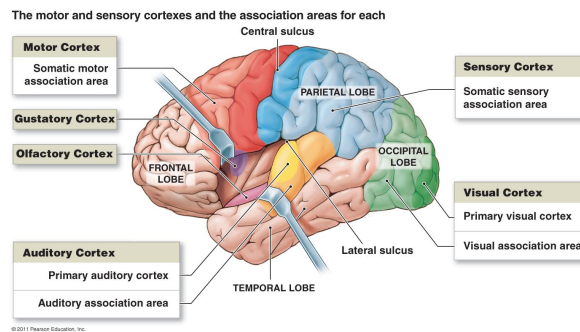


Figure 2.2: The human brain.

## 2.3 K-Nearest Neighbor

## 2.4 The Artificial Deep Neural Networks

The human brain is composed of a big set of specialized cells (*neurons*) connected among them, which memorize and process information, thus controlling the body activities they belong to as depicted in Figure ???. The human brain is probably the most remarkable result of evolution for its ability to elaborate information. The Artificial Neural Networks are mathematical models that represent the interconnection between elements defined "Artificial Neurons", mathematical constructs that somehow imitate the properties of biological neurons, going to reproduce the functioning of the human nervous system.

### 2.4.1 The Human Nervous System

A *biological Neural Networks* is a big set of specialized cells (*neurons*) connected among them, which memorize and process information, thus controlling the body activities they belong to.

The *neuron* model is composed of:

- *Soma*, which is the calculation unit
- *Axon*, that acts as a transmission line output
- *Dendrite* is the input terminal of the cell that receive messages from other connected cells
- *Synapses*: permits a neuron to pass an electrical or chemical signal to another neuron or to the target effector cell.

The *neuron* properties can be described in:

## 2.4 The Artificial Deep Neural Networks

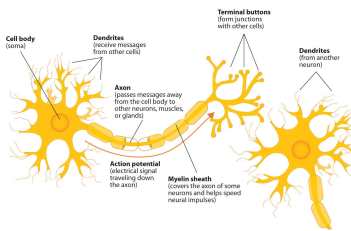


Figure 2.3: The neuron model.

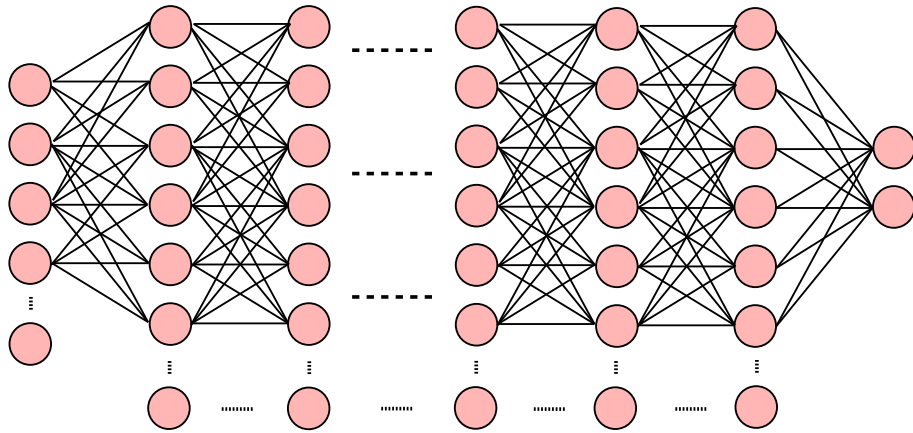
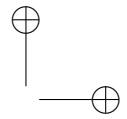
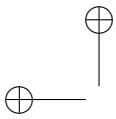


Figure 2.4: The Artificial Neural Network.

- *local simplicity*: the neuron receives stimuli (excitation or inhibition) from dendrites and produces an impulse to the axon which is proportional to the weighted sum of the inputs;
- *global complexity*: the human brain possess  $\mathcal{O}(10^{10})$  neurons, with more than 10K connections each;
- *learning*: even though the network topology is relatively fixed, the strength of connections (synaptic weights) can change when the network is exposed to external stimuli;
- *distributed control*: no centralized control, each neuron reacts only to its own stimuli;
- *tolerance to failures*: performance slowly decrease with the increase of failures.

The biological Neural Networks are able to solve very complex tasks in few time instants (like memorization, recognition, association, and so on.)



## Chapter 2 Background

The *Artificial Neural Networks* (ANNs) are defined as *Massively parallel distributed processors made up of simple processing units having a natural propensity for storing experiential knowledge and making it available for use* (Haykin, 2008).

An ANN resembles the brain in two aspects:

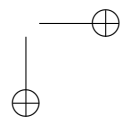
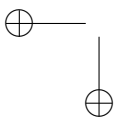
1. Knowledge is acquired by the network from its environment through a learning process;
2. Synaptic weights are used to store the acquired knowledge.

An artificial neural network (ANN), is a mathematical/informatical model calculation based on biological neural networks. This model is constituted by a group of interconnections of information consisting of artificial neurons and processes using a connectionist approach to computation. In most cases, an artificial neural network is an adaptive system that changes its structure, which is based on external or internal information that flows through the network during the learning phase. In practical terms neural networks are non-linear structures of statistical data organized as modeling tools. They can be used to simulate the complex relationships between inputs and outputs that other analytic functions fail to represent. An artificial neural network receives external signals on a layer of nodes (processing unit) input, each of which is connected with a number of internal nodes, organized in several levels. Each node processes the received signals performing a very simple task and transmits the result to subsequent nodes.

The artificial neuron is an information-processing unit that is fundamental to the operation of a neural network. The model of a neuron is composed of three basic elements, as shown in (Figure ??)

- a *set of synapses*, or connecting links, each of which is characterized by a weight or strength of its own,  $w_{km}$ ; The neural model also includes an externally applied *bias*, denoted by  $b_k$ .
- an *adder* for summing the input signals, weighted by the respective synaptic strengths of the neuron; the operations described here constitute a linear combiner;
- an *activation function* for limiting the amplitude of the output of a neuron. Typically, the normalized amplitude range of the output of a neuron is written as the closed unit interval  $[0,1]$ , or, alternatively,  $[-1,1]$ .

The neural model also includes an externally applied *bias*, denoted by  $b_k$ .



## 2.4 The Artificial Deep Neural Networks

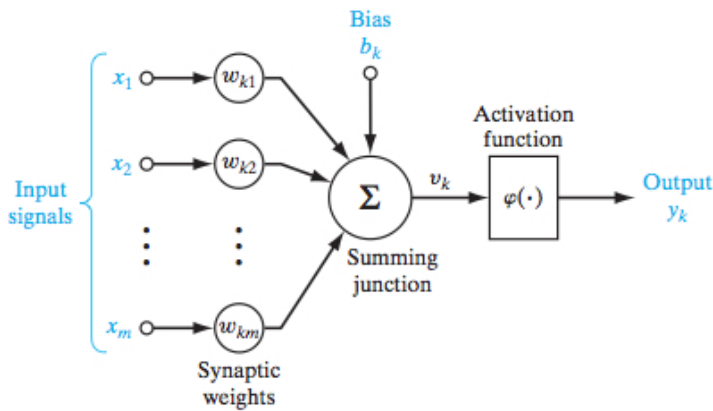


Figure 2.5: The artificial neuron model.

Therefore, the mathematical description of neuron activity can be defined as:

$$u_k = \sum_{j=1}^m w_{kj} x_j \quad (2.21)$$

$$y_k = \varphi(u_k + b_k) \quad (2.22)$$

where:

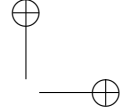
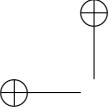
- $x_1, x_2, \dots, x_m$  are the input signals;
- $w_{k1}, w_{k2}, \dots, w_{km}$  are the respective synaptic weights of neuron  $k$ ;
- $u_k$  is the linear combiner output due to the input signals;
- $b_k$  is the bias;
- $\varphi(\cdot)$  is the activation function;
- $y_k$  is the output signal of the neuron.

The types of *activation non-linear functions*  $\varphi(x)$  are:

- the *threshold function*: in engineering, this form of a threshold function is commonly referred to as a Heaviside function;

$$\varphi(v) = 1 \quad \text{if } v \geq 0 \quad (2.23)$$

$$\varphi(v) = 0 \quad \text{if } v < 0 \quad (2.24)$$



## Chapter 2 Background

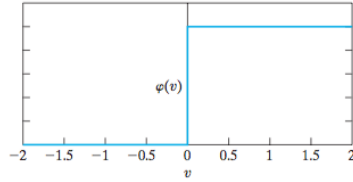


Figure 2.6: The threshold non-linear function.

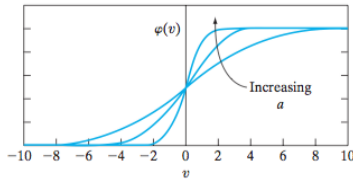


Figure 2.7: The sigmoid non-linear function.

- the *sigmoid function*: it is defined as a strictly increasing function that exhibits a graceful balance between linear and nonlinear behavior; an example of the sigmoid function is the *logistic function* defined by:

$$\varphi(v) = \frac{1}{1 + \exp(-av)} \quad (2.25)$$

- the *hyperbolic tangent (tanh)*: it is simply a scaled and shifted version of the sigmoid function:

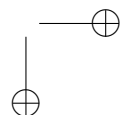
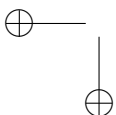
$$\varphi(x) = \frac{1 - e^{-2x}}{1 + e^{-2x}} \quad (2.26)$$

- the *Rectifier Linear Unit (ReLU)*:

$$\varphi(x) = \max(0, x) \quad (2.27)$$

- the *softmax*: it is used on the last layer of a classifier setup: the outputs of the softmax layer represent the probabilities that a sample belongs to the different classes. Indeed, the sum of all the output is equal to 1.

$$\varphi(x_k) = \frac{e^{x_k}}{\sum_{j=1}^N e^{x_j}} \text{ for } k = 1, \dots, K \quad (2.28)$$



## 2.4 The Artificial Deep Neural Networks

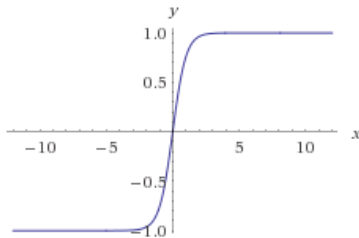


Figure 2.8: The *tanh* non-linear function.

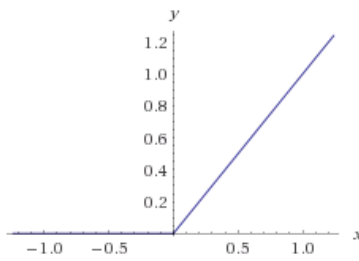


Figure 2.9: The *ReLU* non-linear function.

The manner in which the neurons of a neural network are structured is intimately linked with the learning algorithm used to train the network. There, the *network architectures* (structures) is defined. In general, two different classes of network architectures are identified:

### 1. Multilayer Feedforward Networks - (FFNN):

it is characterized by the presence of one or more hidden layers, whose computation nodes are correspondingly called *hidden neurons* (or hidden units); the term *hidden* refers to the fact that this part of the neural network is not seen directly from either the input or output of the network. The function of hidden neurons is to intervene between the external input and the network output in some useful manner. By adding one or more hidden layers, the network is enabled to extract higher-order statistics from its input.

The MLP is a well known kind of artificial neural network introduced in 1986 [39]. Each node applies an activation function over the weighted sum of its inputs. The units are arranged in layers, with feed forward connections from one layer to the next. The stochastic gradient descent with error back-propagation algorithm is used for the supervised learning of the network. In the forward pass, input examples are fed to the input layer, and the resulting output is propagated via the hidden layers towards the output layer. At the backward pass, the error signal originating

## Chapter 2 Background

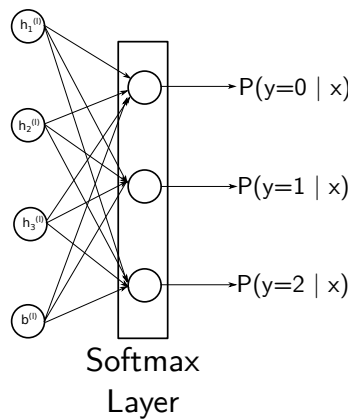


Figure 2.10: The *softmax* layer in a neural network classifier.

at the output neurons is sent back through the layers and the network parameters (i.e., weights and biases) are tuned.

A single neuron can be formally described as:

$$g(\mathbf{u}[n]) = \varphi \left( \sum_{j=1}^D w_j u_j[n] + b \right), \quad (2.29)$$

where  $\mathbf{u}[n] \in \mathbb{R}^{D \times 1}$ , the bias  $b$  is an externally applied term and  $\varphi(\cdot)$  is the non-linear activation function. Thus, the mathematical description of a one-hidden-layer MLP is a function  $\mathbf{f} : \mathbb{R}^D \rightarrow \mathbb{R}^{D'}$ , where  $D'$  is the size of the output vector, so:

$$\mathbf{f}(\mathbf{u}[n]) = \varphi (\mathbf{b}_2 + \mathbf{W}_2 (\varphi (\mathbf{b}_1 + \mathbf{W}_1 \cdot \mathbf{u}[n]))), \quad (2.30)$$

where  $\mathbf{W}_i$  and  $\mathbf{b}_i$  are the respective synaptic weights matrix and the bias vector of the  $i$ -th layer. The behaviour of this architecture is parametrized by the connection weights, which are adapted during the supervised network training.

### 2. Convolutional Neural Networks(CNN)

Convolutional neural networks are feedforward neural networks similar to multilayer perceptron, with some special layers.

Convolution kernels process the input data matrix by dividing it in *local receptive fields*, a region of the same size of the kernel, and sliding the local receptive field across the entire input. Each hidden neuron is thus

#### 2.4 The Artificial Deep Neural Networks

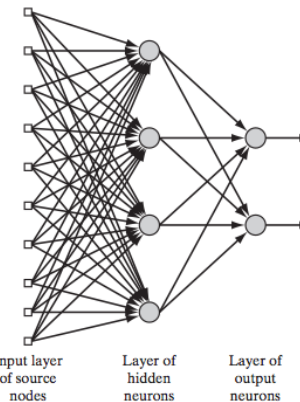


Figure 2.11: The Multilayer Feedforward Network.

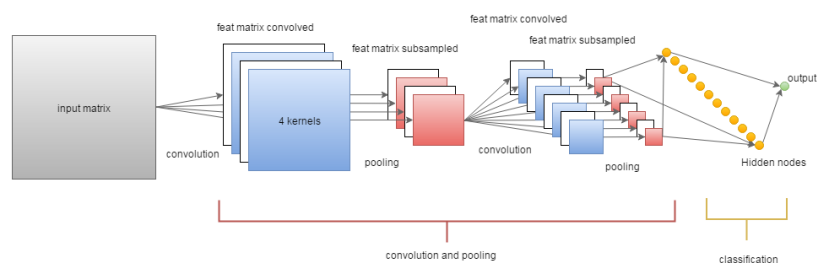


Figure 2.12: The Convolutional Neural Network.

## Chapter 2 Background

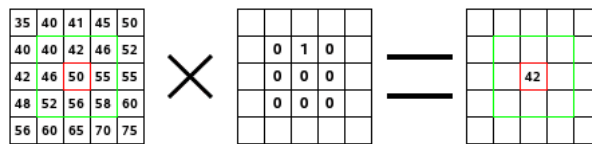


Figure 2.13: The convolution operation.

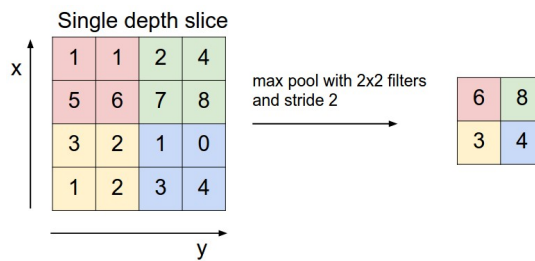


Figure 2.14: The max-pooling layer.

connected to a local receptive field, and all the neurons form a matrix called *feature map*. The weights in each *feature map* are *shared*: all hidden neurons are aimed to detect exactly the same pattern just at different locations in the input image.

The main advantages of this network is the robust pattern recognition system characterized by a strong immunity to pattern shifts.

Pooling layer just reduces the dimension of the matrix by a rule: a submatrix of the input is selected, and the output is the maximum value of this submatrix.

The pooling process introduces tolerance against shifts of the input patterns. Together with convolution layer it allows the CNN to detect if a particular event occurs, regardless its deformation or its position.

CNN is a feed-forward neural network [40] usually composed of three types of layers: convolutional layers, pooling layers and layers of neurons. The convolutional layer performs the mathematical operation of convolution between a multi-dimensional input and a fixed-size kernel. Successively, a non-linearity is applied element-wise. The kernels are generally small compared to the input, allowing CNNs to process large inputs with few trainable parameters. Successively, a pooling layer is usually applied, in order to reduce the feature map dimensions. One of the most used is the *max-pooling* whose aim is to introduce robustness against translations of the input patterns. Finally, at the top of the network, a layer of neurons is applied. This layer does not differ from MLP, being composed

## 2.4 The Artificial Deep Neural Networks

by a set of activation and being fully connected with the previous layer. For clarity, the units contained in this layer will be referred as *Hidden Nodes* (HN).

Denoting with  $\mathbf{W}_m \in \mathbb{R}^{K_{1m} \times K_{2m}}$  the  $m$ -th kernel and with  $\mathbf{b}_m \in \mathbb{R}^{D_1 \times D_2}$  the bias vector of a generic convolutional layer, the  $m$ -th feature map  $\mathbf{h}_m \in \mathbb{R}^{D_1 \times D_2}$  is given by:

$$\mathbf{h}_m = \varphi \left( \sum_{d=1}^{D_3} \mathbf{W}_m * \mathbf{u}_d + \mathbf{b}_m \right), \quad (2.31)$$

where  $*$  represent the convolution operation, and  $\mathbf{u}_d \in \mathbb{R}^{D_1 \times D_2}$  is a matrix of the three-dimensional input tensor  $\mathbf{u} \in \mathbb{R}^{D_1 \times D_2 \times D_3}$ . The dimension of the  $m$ -th feature map  $\mathbf{h}_m$  depends on the zero padding of the input tensor: here, padding is performed in order to preserve the dimension of the input, i.e.,  $\mathbf{h}_m \in \mathbb{R}^{D_1 \times D_2}$ . Please note that for the sake of simplicity, the time frame index  $n$  has been omitted. Commonly, (2.31) is followed by a pooling layer in order to be more robust against patterns shifts in the processed data, e.g. a max-pooling operator that calculates the maximum over a  $P_1 \times P_2$  matrix is employed.

A *Deep Learning* definition: *A class of machine learning techniques that exploit many layers of non-linear information processing for supervised or unsupervised feature extraction and transformation, and for pattern analysis and classification.* Artificial Neural Networks are often referred as deep when they have more than 1 or 2 hidden layers.

### 2.4.2 Stochastic gradient descent (SGD)

Most deep learning training algorithms involve optimization of some sort. The most widely used is the gradient based optimization, which belongs to the first order type.

*Optimization* is the task of either minimizing some function  $f(x)$  by altering  $x$ :  $f(x)$  is called *objective function*, but in the case when it has to be minimized, it is also call the *cost function*, *loss function*, or *error function*. The aim of the optimization is reached doing small change  $\epsilon$  in the input  $x$ , to obtain the corresponding change in the output  $f(x)$ :

$$f(x + \epsilon) \approx f(x) + \epsilon f'(x). \quad (2.32)$$

This formulation is based on the calculation of the derivative  $f'(x)$ . The *gradient descent* is the technique based on the reduction of  $f(x)$  by moving  $x$  in small steps with the opposite sign of the derivative. The aim is to find the minimum

## Chapter 2 Background

of the cost function: when  $f''(x) = 0$ , the derivative provides no information about which direction to move, therefore this point is defined as stationary points. A local minimum is a point where  $f(x)$  is lower than at all neighbouring and it is no longer possible to decrease  $f(x)$  by making infinitesimal steps. The absolute lowest value of  $f(x)$  is a *global minimum*.

For the concept of minimization to make sense, there must still be only one (scalar) output. For functions that have multiple inputs  $f : \mathbb{R}^n \rightarrow \mathbb{R}$ , the concept of *partial derivatives* is introduced. The gradient  $\nabla_{\mathbf{x}} f(\mathbf{x})$  is the vector containing all the partial derivatives.

The method of *steepest descent* or *gradient descent* states that decrease  $f$  by moving in the direction of the negative gradient.

$$\mathbf{x}' = \mathbf{x} - \epsilon \nabla_{\mathbf{x}} f(\mathbf{x}), \quad (2.33)$$

where  $\epsilon$  is the *learning rate*, a positive scalar determining the size of the step.

Large training sets are necessary for good generalization, but large training sets are also more computationally expensive. The cost function decomposes as a sum over training example of per-example loss function: i.e., the negative conditional log-likelihood of the training data is defined as:

$$J(\theta) = \mathbb{E}(L(\mathbf{x}, y, \theta)) = \frac{1}{m} \sum_{i=1}^m L(\mathbf{x}^{(i)}, y^{(i)}, \theta), \quad (2.34)$$

where  $L$  is the per-example loss  $L(\mathbf{x}, y, \theta) = -\log p(y|\mathbf{x}; \theta)$ . The gradient descent requires computing:

$$\nabla_{\theta} J(\theta) = \frac{1}{m} \sum_{i=1}^m \nabla_{\theta} L(\mathbf{x}^{(i)}, y^{(i)}, \theta). \quad (2.35)$$

The computational cost of this operation is proportional to the number of example  $m$ , therefore as the training set size grows the time to take a single gradient step becomes prohibitively long.

*Stochastic gradient descent* (SGD) is an extension of the gradient descent algorithm: the insight is that the gradient is an expectation estimated using a small set of samples. On each step of the algorithm, a sample of example  $\mathbb{B} = \{\mathbf{x}^{(1)}, \dots, \mathbf{x}^{(m')}\}$ , called *minibatch*, is drawn uniformly from the training set. The minibatch size  $m'$  is typically chosen to be a relatively small number of examples. The estimate of the gradient is:  $\mathbf{g} = \frac{1}{m'} \nabla_{\theta} \sum_{i=1}^{m'} L(\mathbf{x}^{(i)}, y^{(i)}, \theta)$  using examples from the minibatch  $\mathbb{B}$ . The SGD algorithm then follows the estimated gradient downhill:

$$\theta \leftarrow \theta - \epsilon \mathbf{g} \quad (2.36)$$

## 2.4 The Artificial Deep Neural Networks

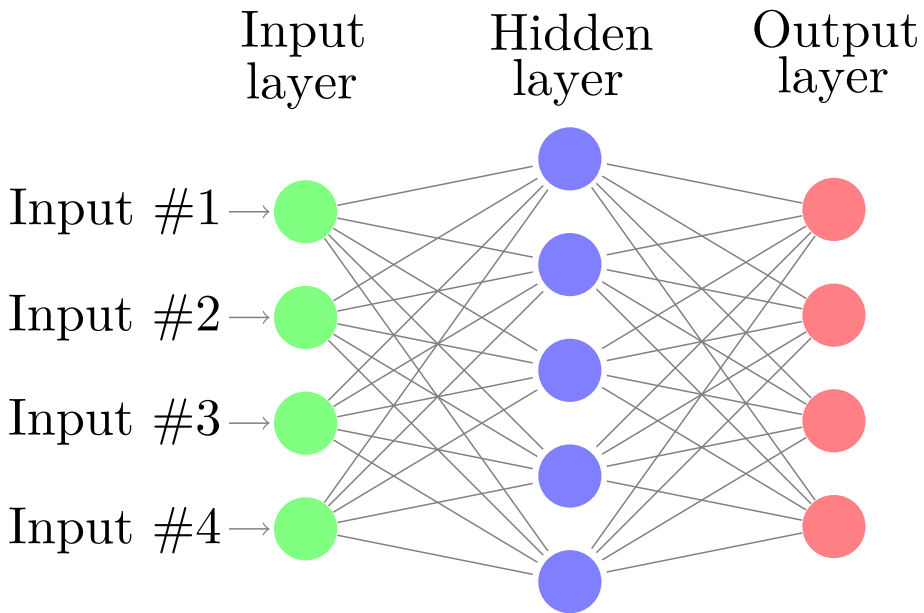


Figure 2.15: The different types of Autoencoders.

where  $\epsilon$  is the learning rate.

### 2.4.3 Autoencoder

An Autoencoder is a kind of neural network typically consisting of only one hidden layer, trained to set the target values to be equal to the inputs.

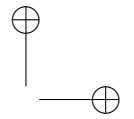
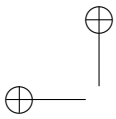
$$\tilde{x} = f(W_2 h(x) + b_2) \quad (2.37)$$

Given an input set of examples  $\mathcal{X}$ , autoencoder training consists in finding parameters  $\theta = \{W_1, W_2, b_1, b_2\}$  that minimize the Reconstruction Error:

$$\mathcal{J}(\theta) = \sum_{x \in \mathcal{X}} \|x - \tilde{x}\|^2 \quad (2.38)$$

Defining  $M$  the number of hidden units, and  $N$  the number of input units, output units, features size:

- (a):  $M = N \rightarrow$  Basic Autoencoder (AE);
- (b):  $M < N \rightarrow$  Compression Autoencoder (CAE);
- (c):  $M > N$  and Gaussian Noise  $\rightarrow$  Denoising Autoencoder (DAE);



## Chapter 2 Background

An AE – a kind of neural network typically consisting of only one hidden layer –, sets the target values to be equal to the input. It is used to find common data representation from the input [41, 42]. Formally, in response to an input example  $x \in \mathbf{R}^n$ , the hidden representation  $h(x) \in \mathbf{R}^m$  is

$$h(x) = f(W_1x + b_1), \quad (2.39)$$

where  $f(z)$  is a non-linear activation function, typically a logistic sigmoid function  $f(z) = 1/(1+\exp(-z))$  applied component-wisely,  $W_1 \in \mathbf{R}^{m \times n}$  is a weight matrix, and  $b_1 \in \mathbf{R}^m$  is a bias vector.

The network output maps the hidden representation  $h$  back to a reconstruction  $\tilde{x} \in \mathbf{R}^n$ :

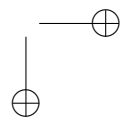
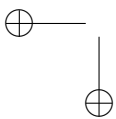
$$\tilde{x} = f(W_2h(x) + b_2), \quad (2.40)$$

where  $W_2 \in \mathbf{R}^{n \times m}$  is a weight matrix, and  $b_2 \in \mathbf{R}^n$  is a bias vector.

Given an input set of examples  $\mathcal{X}$ , AE training consists in finding parameters  $\theta = \{W_1, W_2, b_1, b_2\}$  that minimise the reconstruction error, which corresponds to minimising the following objective function:

$$\mathcal{J}(\theta) = \sum_{x \in \mathcal{X}} \|x - \tilde{x}\|^2. \quad (2.41)$$

The minimisation is usually realised by stochastic gradient descent as in the training of neural networks. The structure of the AE is given in Figure 2.15a.



# Chapter 3

## Dataset

The importance of using public data sets for algorithm evaluation is very important. Only in this way can a direct comparison be made between the different approaches to determine which of these is actually the best. There are publicly available datasets for the fall detection task, the majority of them are all related to wearable or vision sensors and often include both types [43, 44, 45, 46, 47]. Since in this work, we face the problem fall detection from an audio perspective, only one dataset containing audio recording has been found [48]. However, the audio files available in the dataset are suitable for speech recognition related works rather than sound event detection. In fact, only the utterance of short sentences or interjections of the actors involved during the human falls recordings have been annotated. As in this work, several data-driven approaches for pattern recognition produced by the sound generated by the human fall are presented, the dataset [48] result useless. Given the lack of available audio data sets, we have created a suitable audio dataset in order to assess the proposed approaches. This choice was also forced by the fact that in these works an innovative acoustic sensor was explicitly developed for the fall detection and described in Section 3.1 has been used. In this chapter, the instrumentation, the procedure for recording the audio corpus and its composition are described.

### 3.1 The floor acoustic sensor

The floor acoustic sensor (FAS) is composed of a resonant enclosure and a microphone located inside it (Figure 3.1) [49]. At the bottom of the enclosure, a membrane is in direct contact with the floor and guarantees the acoustic coupling with the surface. The inner container accommodates the microphone and is where the acoustic resonance phenomenon takes place. It can be covered by a layer of acoustic isolation material and it is enclosed by the outer container that further reduces the intensity of the acoustic waves that propagate through air. The enclosure has been manufactured in Polylactic Acid with a 3D printer, its diameter is 16.5 cm and its height 5.5 cm.

### Chapter 3 Dataset

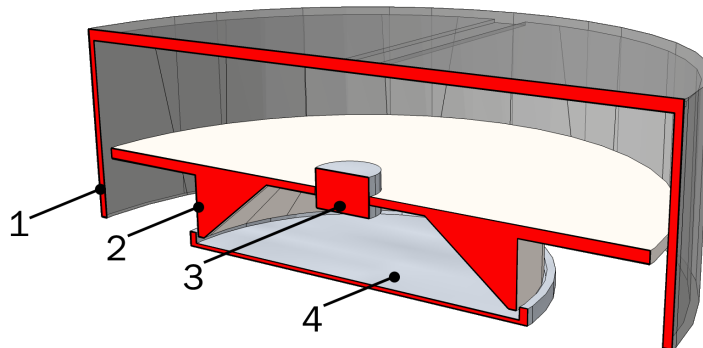


Figure 3.1: The floor acoustic sensor: conceptual scheme. 1 - The outer container. 2 - The inner container. 3 - The microphone slot. 4 - The membrane touching the floor.

Regarding the microphone, an AKG C 400 BL<sup>1</sup> has been inserted in the enclosure. The outer case of the microphone has been removed to extract the capsule that has then been inserted in the sensor enclosure. The AKG C 400 BL is characterized by an hypercardiod directivity pattern, thus it has been oriented so that the maximum gain is towards floor.

## 3.2 The fall events dataset: A3Fall

The performance of the floor acoustic sensor has been evaluated on a corpus of audio events corresponding to falls of several objects recorded in different conditions<sup>2</sup>. The dataset has been specifically created by the authors and it will be presented in this section.

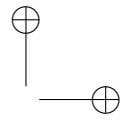
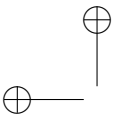
### 3.2.1 The recording setup

Fall events have been recorded in 3 different rooms with the following characteristics:

- The first, is a rectangular room, hereafter named R0, measuring about 7 m × 2 m (Figure 3.5). The room is particularly suitable for the propagation of acoustic waves through the floor since it is obtained from a cantilever beam. In addition, the considerable distance of the supporting pillars facilitates the transmission of a fall vibrations through the floor.

<sup>1</sup><http://www.akg.com/pro/p/c400-bl>

<sup>2</sup>The dataset is available at the following URL: <http://www.a3lab.dii.univpm.it/research/fasdataset>



### 3.2 The fall events dataset: A3Fall



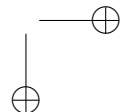
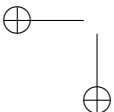
Figure 3.2: A picture of the floor acoustic sensor used during the recordings.

- the second location for the recording was the university auditorium room (R1) in which the flooring is composed of fitted carpet. This makes it particularly suitable for evaluating system performance on surfaces with acoustical behavior that can mitigate the impact sound transmitted through the floor and in the air; all the recordings were performed near the auditorium stage in an area of 8×3 m.
- a recording studio (R2) was selected as the third location for its particular characteristics. Here, it was possible to make the acquisitions by placing the sensors in the live room while the audio events were performed in the control room. In particular, the sensors were positioned immediately behind the soundproof wall with the window overlooking the live room. The size of the live room is 5×7 m, while the size of the control room is 3×8 m.

The recording equipment comprises the floor sensor, a linear array of three aerial microphones (the same AKG 400 BL included in the floor sensor) and a Presonus AudioBox 44VSL sound card connected to a laptop. The microphones of the array are separated by 4 cm and positioned on a table 80 cm high. Signals were sampled at 44.1 kHz with a resolution of 32 bits. Levels were calibrated to assure the maximum dynamic range at the smallest distance.

#### 3.2.2 Description

In Table 3.1 the composition of the dataset is summarized. For the R0, the dataset comprises recordings of fall events related to everyday objects and to



### Chapter 3 Dataset

Table 3.1: Composition of the A3Fall-v2.0 dataset.

Class	R0	R1	R2
	Nr. of occurrences		
Basket	64	40	40
Fork	64	40	40
Ball	64	40	40
Book	64	40	40
Bag	64	30	40
Chair	96	40	40
Table	0	40	40
Guitar Slide	0	40	40
Nipper	0	40	40
Keys	0	40	40
Hook	0	40	40
Coat Hook	0	40	40
Manikin Doll	44	0	0
Human Fall	0	40	40
	Total length (s)		
Background	2530	9055	5550

a human mimicking doll. The objects were chosen according to the recent literature on the topic [27] and are the following: a ball, a metal basket, a book, a metal fork, a plastic chair, and a bag (Figure 3.3). Objects have been dropped at four distances from the sensors, i.e., 1 m, 2 m, 4 m, and 6 m, and with various angles in order to reproduce realistically different fall patterns. With the exception of the chair and the basket, which have been overturned from their natural position, half of the falls has been performed at a height of 0.5 m and the other half at 1 m. For each object and for each distance, 16 fall events have been performed for a total of 64 events per object. Instead, the chair has been overturned 8 times for each side of fall (back, front, side) and for each distance, thus obtaining a total of 96 events.

Human falls have been simulated by employing the “Rescue Randy” doll<sup>3</sup>, a professional equipment employed in water rescues. It weights 75 kg, it is 1.85 m high, and it is equipped with articulated joints. The doll is made of vinyl and its weight is distributed according to the human weight distribution chart. The doll has been dropped from upright position and from a chair, both forward and backward, for a total of 44 events (Figure 3.4). Differently from the everyday objects, the distribution of the fall events with the distance is not uniform: 10 events have been performed from 2 m, 18 from 4 m (7 of which from the chair),

<sup>3</sup><http://www.simulaids.com/1475.htm>

### 3.2 The fall events dataset: A3Fall



Figure 3.3: Objects employed for creating the fall events dataset.

and 16 from 6 m (6 of which from the chair).

Moreover, several background sounds have been added to the dataset. Normal activities sounds have been recorded while persons were performing common actions, such as walking, talking, and dragging chairs. Three musical tracks have been played from a loudspeaker and acquired back with the FAS. The first track contained classical music<sup>4</sup>, while the second<sup>5</sup> and the third<sup>6</sup> rock music. Musical tracks and normal activities sounds have been divided in segments whose lengths have mean and standard deviation estimated from instances of fall events. In addition, they have been employed alone and to create noisy versions of human and object falls occurrences in order to assess the algorithm in presence of interferences.

In R2 and R1 other every-days objects, in addition to those used in R0, have been recorded for a total of 12 different object fall classes and 1420 instances. While the manikin doll has been used only in R0, in R1 and R2 a total 80 human falls have been performed by 4 people. These falls were performed in different ways: forward, backward and on the side, trying to use the arms to cushion the fall and without any protections. As in R0, also in R2 and R2 all events were performed from 1, 2, 4 and 6 m away from the FAS.

As shown in Table 3.1 background noises have been recorded also in R1 and R2 rooms, which include: human activities noise as, i.e., footsteps, human and phone conversation, dragging objects and so on; classic, rock and pop music played from loudspeakers; TV shows like newscast and satiric.

Since the data relating to rooms R1 and R2 have been collected at different times to those of room R0, in the following chapters, for each proposed ap-

<sup>4</sup>W. A. Mozart, “Piano trio in C major”

<sup>5</sup>Led Zeppelin, “Dazed and confused”

<sup>6</sup>Led Zeppelin, “When the levee breaks”

### Chapter 3 Dataset



(a) Fall from upright position. (b) Fall from the chair.

Figure 3.4: Falls of the “Rescue Randy” doll from upright position (a) and from the chair (b).

proach, it will be specified which subset of the total dataset has been used as well as the usage of the noisy version of falls events.

#### 3.2.3 Signal analysis

The signal related to the same fall event acquired with the floor sensor and with the aerial microphone exhibits different spectral characteristics. In this section and in depth analysis of the audio signals acquired in the R0 room is presented. Figure 3.6 shows the spectrograms of a doll fall acquired with the floor sensor (above) and with the aerial microphone (below) in the clean acoustic condition. Observing the figures, it can be noticed that the aerial microphone is more sensitive to high frequencies, in particular to the ones above 1.5 kHz. On the contrary, the majority of the energy of the signal acquired with the floor sensor concentrates below 1 kHz.

This is even more evident by plotting the values of the mel coefficients (Figure 3.7): the first and second mel channels of the FAS, corresponding to the frequency bands 0–128.10 Hz and 61.30–200.60 Hz, are higher respect to the aerial microphone. Channels 3 to 7, respectively corresponding to bands 128.10–279.50 Hz and 458.70–670.70 Hz, are almost equivalent, while from channel 8 (560.30–790.80 Hz) to 29 (6654.60–8000.00 kHz) the aerial microphone mels are greater.

The analysis of noisy signals highlights the different behaviour of the floor sensor respect to the aerial microphone in presence of external interferences.

### 3.2 The fall events dataset: A3Fall

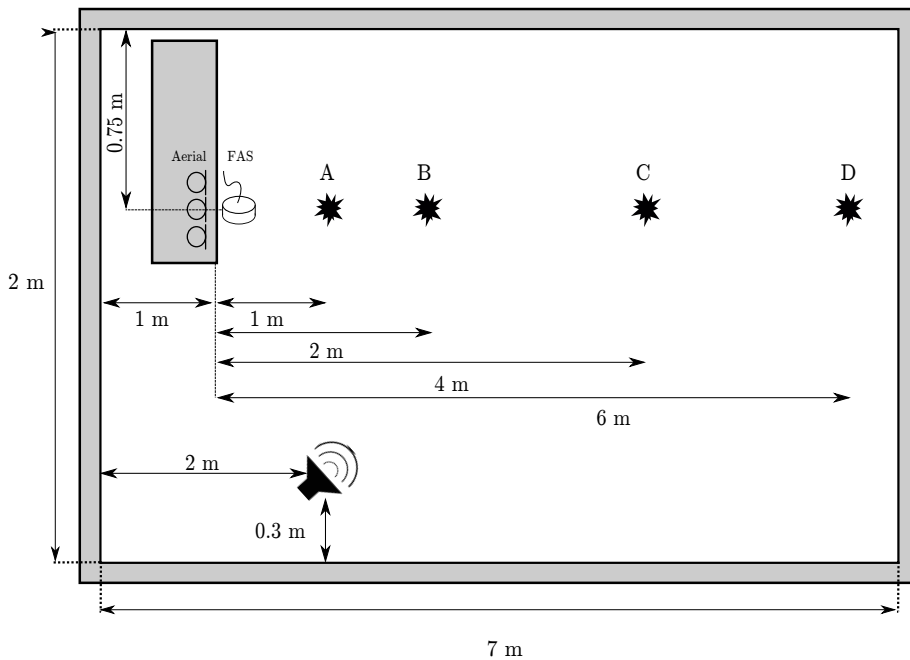
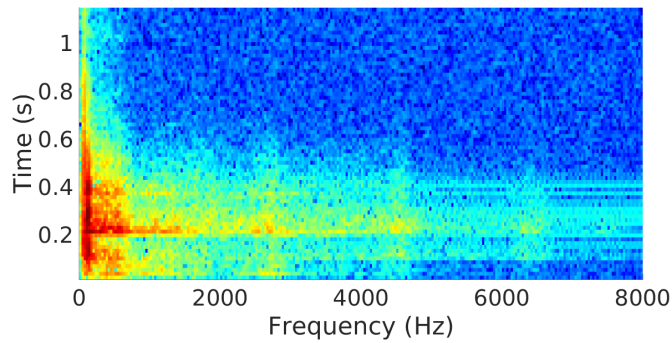


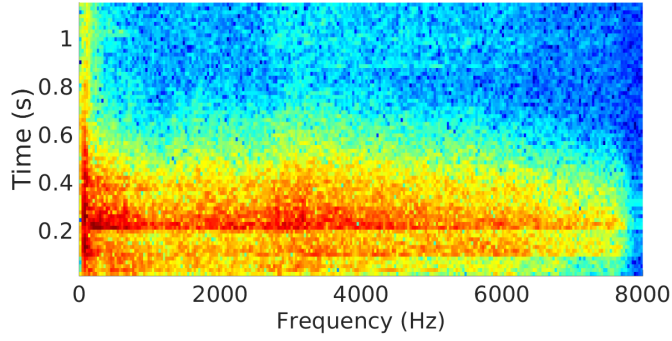
Figure 3.5: The recording room: the letters A, B, C and D indicate the positions of fall events.

In fact, taking into account the backgrounds tracks as interferences, the floor sensor has a global signal-to-noise ratio (SNR) equal to 20.94 dB and a segmental SNR equal to 7.28 dB. The global SNR of the central aerial microphone is 8.92 dB and the segmental SNR is -1.47 dB. The values of the aerial microphone SNRs are thus considerably lower than the ones of the floor sensor. The global SNR of the floor sensor noisy dataset is 13.66 dB higher than the one of the aerial microphone, highlighting the superior ability of the former to isolate fall signals from external interferences. However, it is worth investigating how the SNR distributes over the frequency range of the acquired signals in order to have a better insight of the physical phenomenon. Figure 3.8 shows the SNR calculated for each mel channel and averaged across the noisy datasets. It can be noticed that the SNR of the floor sensor exceeds the one of the aerial microphone for channels below the fourth. Then, the opposite occurs and the SNR of the aerial microphone assumes greater values. The “valley” in the curves are due to the pitch of the music signal.

Chapter 3 Dataset



(a) Spectrogram of the signal acquired with the floor sensor.



(b) Spectrogram of the signal acquired with the aerial microphone.

Figure 3.6: Frequency content of the same fall event (file “rndy\_d2st\_bar\_0.wav”) acquired with the FAS (a) and with the aerial microphone (b).

### 3.2 The fall events dataset: A3Fall

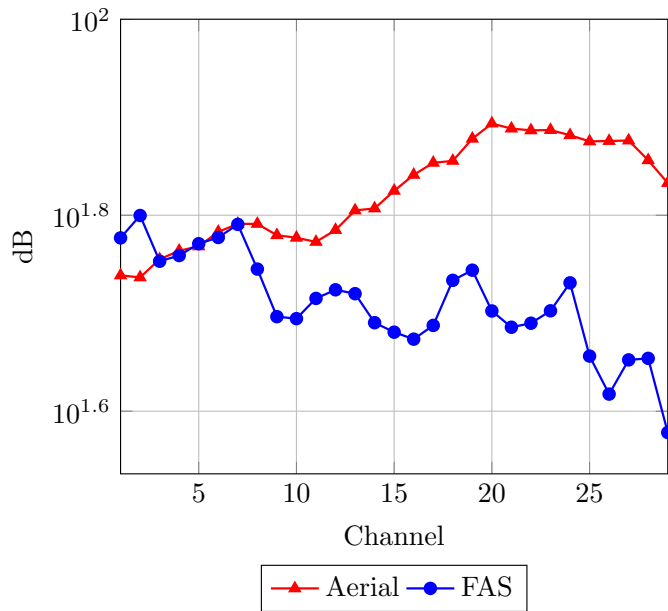


Figure 3.7: Average value of the mel channels.

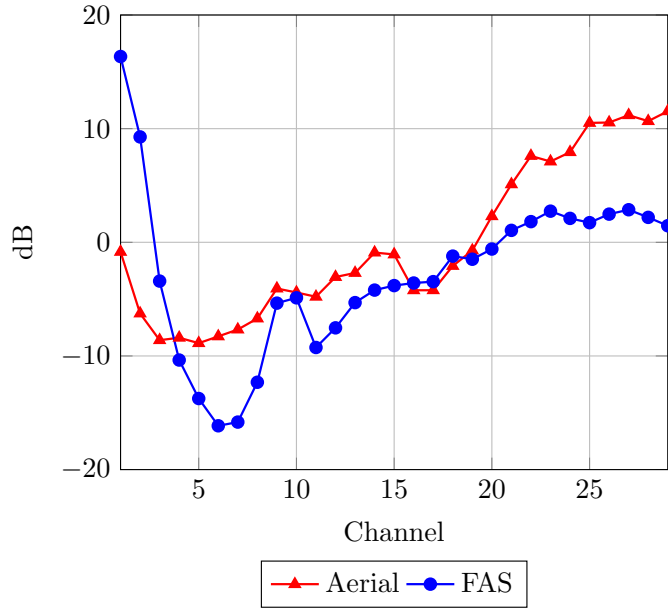
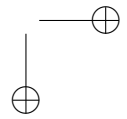
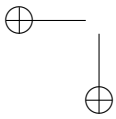
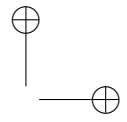
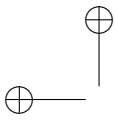
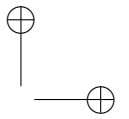
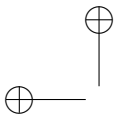


Figure 3.8: Average value of the SNR for each mel channel.





# Chapter 4

## Supervised Approach

qua vengono presentati sia il metodo multilabel classifier GMM-UBM SVM (ESWN) che il binary GMM-UBM SVM (WIRN2016)

### 4.1 Support-Vector Machine based algorithm for evens fall classification

The fall detection task consists in recognize which object produced the pattern of a signal and it mainly consists of two subtasks: the location of the time boundaries of the fall event and the classification of that event. In this section, we concentrate on the second subtask, since the main objective is determining the performance of the acoustic sensor as compared to common aerial microphones. The entire falls detection activity will be addressed in the works presented below.

#### 4.1.1 Proposed approach

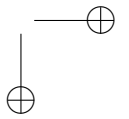
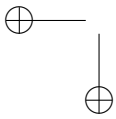
The fall classification algorithm is composed of a feature extraction stage and a classification stage. The first extracts MFCCs from the input audio signal, while the second classifies the audio event by means of Gaussian means supervectors and SVM. Following is a detailed description of the two stages.

##### Feature extraction

Despite MFCCs were originally developed for speech and speaker recognition tasks, they have been successfully applied also for acoustic event classification [50] and fall detection [16].

The block-scheme of the MFCC feature extraction pipeline is shown in Figure 4.1. The first processing step is the pre-emphasis of the input signal, which consists in applying a filter whose transfer function is:

$$G(z) = 1 - \alpha z^{-1}. \quad (4.1)$$



#### Chapter 4 Supervised Approach

Usually  $0.9 < \alpha \leq 1.0$  and here it has been set to 0.97. The objective of pre-emphasis is to remove the DC components and to raise the high-frequency part of the spectrum.

The signal is then segmented in frames 16 ms long overlapped by 8 ms and multiplied with a Hamming window. For each frame, the Discrete Fourier Transform (DFT) is calculated and filtered with a filterbank composed of 29 triangular filters uniformly spaced on the mel scale.

Denoting with  $S(i)$  the DFT of a frame and  $i$  the frequency bin, the output of the “Mel Filterbank & Frequency Integration” block in Figure 4.1 is

$$mel(k) = \sum_{i=ini(k)}^{end(k)} |S(i)|^2 W_k(i), \quad k = 1, 2, \dots, N \quad (4.2)$$

where  $mel(k)$  is the energy of the  $k$ -th subband,  $W_k(i)$  is the frequency response of the  $k$ -th filter,  $ini(k)$  and  $end(k)$  are starting and ending frequency indices of that filter and  $N$  is the number of filters in the bank, which in this case is 29. The terms  $mel(k)$  are often named “mel coefficients”.

The final steps for the calculation of the  $j$ -th MFCC  $c(j)$  is the logarithm and the Discrete Cosine Transform (DCT):

$$c(j) = \sum_{k=1}^N \log[H(k)] \cos\left[\frac{\pi j}{N}(k - 0.5)\right], \quad j = 0, 1, \dots, M - 1 \leq N \quad (4.3)$$

The set  $\{c(0), c(1), \dots, c(M - 1)\}$  forms the static coefficients elements of the feature vector. Here  $M$  has been set to 13. The final feature vector is composed of 39 coefficients, i.e., the 13 static coefficients plus their first and second derivatives.

#### Classification stage

The approach proposed in this section is based on a One-Class Support Vector Machine (OCSVM) [37]. The general idea is that a human fall produces a

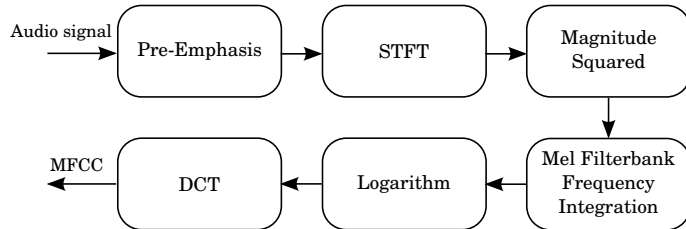


Figure 4.1: The MFCC feature extraction pipeline.

#### 4.1 Support-Vector Machine based algorithm for evens fall classification

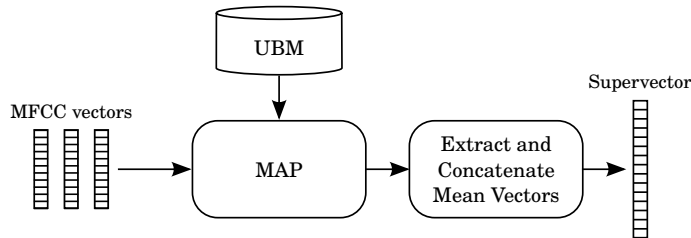


Figure 4.2: Block scheme for extracting a gaussian mean supervector from MFCCs and a trained UBM.

sound considerably different from the ones commonly occurring in a home (e.g., voices, sounds from electronic devices, footsteps, etc.). The OCSVM is trained on a large set of “normal” sounds to detect acoustic events that deviate from normality. However, it is expected that certain acoustic events are as abnormal as a human fall (e.g., the fall of book, a chair, etc.), thus they could raise false alarms.

The classification stage employs Gaussian Mean Supervectors (GMS) and a Support Vector Machine classifier as in speaker recognition systems [51]. The algorithms consists in modelling the entire acoustic space with a Universal Background Model (UBM) represented by mixture of gaussians (Gaussian Mixture Model, GMM). The GMM is trained using the Expectation Maximization (EM) algorithm [52] on a large corpus of acoustic events. Then, for each acoustic event class in the training corpus a GMS is calculated by adapting the UBM with the Maximum A Posteriori (MAP) algorithm [53] and concatenating the adapted GMM mean values. The block diagram of the approach is shown in Figure 4.2. The final step of the training phase is the estimation of the SVM parameters. In this work, an SVM with a radial basis function has been used. The complete diagram of the training phase is shown in Figure 4.3.

Classification is performed by extracting the supervector from an input audio signal as in the training phase, and then determining the acoustic event class evaluating the SVM discriminant function (Figure 4.4). Since the number of classes is greater than two and SVMs are binary classifiers, the “one versus all” technique has been adopted [35]. LIBSVM [54] has been employed both in the training and testing phases of the SVM.

##### 4.1.2 Dataset

All the experiments have been conducted data related to R0 room only. In particular, in order to compare the performance of the FAS with a standard aerial microphone, not all data concerning all the aerial microphones array have been used but only the one of the microphone closest to the wall (see Figure 3.5).

#### Chapter 4 Supervised Approach

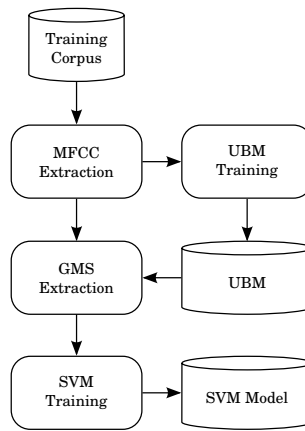


Figure 4.3: Block scheme for training the UBM and SVM models.

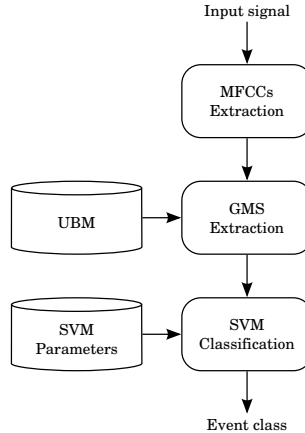


Figure 4.4: Block-scheme of the fall classification phase.

Moreover, signals have been downsampled to 16 kHz and the resolution has been reduced to 16 bit. In order to obtain a balanced dataset, for each object and for each distance, 11 fall events have been randomly picked for a total of 44 events per object, while all the 44 simulated human fall with the manikin has been selected. In addition, the three musical track recorded in the R0 room have been employed to create a noisy version of the dataset by digitally adding a random segment of the recorded musical tracks to the “clean” datasets as was done for the analysis of the signals in Section 3.2.3. In particular, the analysis presented in Section 3.2.3 suggested the authors that the standard MFCC extraction pipeline can be modified in order to better exploit the properties the floor acoustic sensor. In particular, the analysis led to the following considerations:

- The pre-emphasis filter is an inheritance of automatic speech recognition

#### 4.1 Support-Vector Machine based algorithm for evens fall classification

Table 4.1: Data related to R0 room used in this work.

Classes	Nr. of occurrences
Basket	44
Fork	44
Ball	44
Book	44
Bag	44
Chair	44
Manikin Doll	44
Backgrounds	Total length (s)
Classic Music	882
Rock Music	616

systems, where the input signal is the human voice. Since the effect of the filter is to enhance the high frequency components of the signal and the floor sensor is more sensitive to low frequencies, removing the pre-emphasis could improve the classification performance.

- The majority of the energy of the signals acquired with the floor acoustic sensor is concentrated at frequencies below 1.5 kHz. This suggest that introducing a low-pass filter that removes low SNR frequencies may improve the classification performance.

In Table 4.1 the data used for this approach are summarized.

#### 4.1.3 Experimental setup

The MFCC extraction pipeline has been firstly parametrised as described in Section 4.1.1, then, based on the study presented in the previous section, two additional pipelines have been tested:

- no pre-emphasis (NOPRE): the pre-emphasis stage has been removed from the feature extraction pipeline;
- no pre-emphasis plus low-pass filtering (NOPRELP): the pre-emphasis stage has been removed and the maximum frequency of the mel filterbank has been set to 4 kHz.

The standard MFCC extraction pipeline described in Section 4.1.1 will be denoted with “STD” in the results.

Regarding the UBM, it has been trained until convergence with the EM algorithm setting the threshold value to  $10^{-3}$ . The same value has been employed

## Chapter 4 Supervised Approach

in the MAP adaptation algorithm, but the maximum number of iterations was set to 5.

Due to the limited amount of data, the experiments have been conducted with the leave-one-label-out method: fall events recorded at all distances but one were employed for training and validation, while the remaining for testing. The validation phase consisted in searching for the number of components of the UBM and for the SVM hyperparameters which yielded the best results. In particular, the number of components of the UBM assumed the values  $\{1, 2, \dots, 64\}$ , while the SVM hyperparameters  $C$  and  $\gamma$  the values  $\{2^{-5}, 2^{-3}, \dots, 2^{15}\}$  and  $\{2^{-15}, 2^{-13}, \dots, 2^3\}$  respectively.

The performance was evaluated both on clean data and on data corrupted with the music interference. In particular, the system was evaluated in matched condition, where the acoustic scenario of the training, validation and test data is the same, in mismatched condition, where training data is clean and testing data is corrupted with music, and in multi-condition, where training data and testing data contain both clean signals and corrupted signals. In the latter case, the training, validation and test sets have been divided so that they contain 1/3 of clean data and 2/3 of noisy data.

The performance has been evaluated in terms of precision ( $P$ ), recall ( $R$ ) and  $F_1$ -Measure ( $F$ ) per class and the values have then been averaged. The metrics definitions for class  $i$  is:

$$P_i = \frac{C(i, i)}{\sum_j C(j, i)}, \quad (4.4)$$

$$R_i = \frac{C(i, i)}{\sum_j C(i, j)}, \quad (4.5)$$

$$F_i = \frac{2P_i R_i}{P_i + R_i}, \quad (4.6)$$

where  $C = [C(i, j)]$  is the confusion matrix.

### 4.1.4 Results

#### Results in matched condition

Figure 4.5 shows the results obtained in matched condition. As shown in the figure, the FAS exceeds the  $F_1$ -Measure of the aerial microphone both with clean and noisy signals regardless the feature setup employed. In particular, in clean conditions the aerial microphone achieves the highest  $F_1$ -Measure with standard MFCCs, while the FAS with the NOPRELP ones, which results in 6.50% absolute improvement. In noisy conditions, the aerial microphones best performance is again achieved with STD features, while the FAS one is achieved with the NOPRE features, with the NOPRELP setup performing almost the

#### 4.1 Support-Vector Machine based algorithm for evens fall classification

Table 4.2: Aerial microphone confusion matrix related to the STD configuration in clean condition. The average precision is 91.48%, the average recall 91.23%, and the average F<sub>1</sub>-Measure 91.04%.

	Doll	Bag	Ball	Basket	Book	Chair	Fork	F <sub>1</sub>
Doll	93.18	0	0	0	2.27	4.55	0	90.11
Bag	0	86.36	0	0	13.64	0	0	82.61
Ball	0	0	100.00	0	0	0	0	100.00
Basket	2.27	0	0	97.73	0	0	0	98.85
Book	0	22.73	0	0	77.27	0	0	78.16
Chair	11.36	0	0	0	4.55	84.09	0	89.16
Fork	0	0	0	0	0	0	100	100.00
Precision	87.27	79.17	100.00	100.00	79.07	94.87	100.00	

same. The absolute improvement of the FAS respect to the aerial microphone is 5.36%.

Focusing on the FAS performance with the various feature extraction pipelines, the highest F<sub>1</sub>-Measure is obtained by removing the pre-emphasis and low-pass filtering the signals (NOPRELP) in clean conditions. Notice, however, the standard pipeline performs almost the same, thus in this condition the influence is minimal. The sole removal of the pre-emphasis, on the other hand, is detrimental for the classification performance. The opposite occurs in noisy condition, where the removal of the pre-emphasis improves the results by 3.99%. Low-pass filtering, on the other hand, does not give further improvements. Overall, the feature pipeline that gives the highest F<sub>1</sub>-Measure is the NOPRELP, as argued in Section 3.2.3.

Further insights on the results are given by the confusion matrices of the aerial microphone (Table 4.2) and of the FAS (Table 4.3) for the feature pipeline giving the highest F<sub>1</sub>-Measure. With the only exception of the basket falls, the FAS is able to achieve superior performance for all the objects in the dataset. In particular, the doll F<sub>1</sub>-Measure improves by 9.89% respect to the aerial microphone. The object exhibiting the lowest performance regardless the sensor is the book: this can denote a limit in the algorithm suggesting that further improvements could be obtained by properly modifying the features or the classifier.

#### Results in mismatched condition

Figure 4.6 shows the results obtained in mismatched condition, i.e., with training and validation performed on clean data and testing on noisy data. As expected, both the performance of the aerial microphone and of the floor sensor decrease. Notice, however, that regardless the features employed, the floor sensor is able to achieve considerably higher F<sub>1</sub>-Measures respect to the aerial microphone. In particular, the floor sensor highest F<sub>1</sub>-Measure, obtained with

## Chapter 4 Supervised Approach

Table 4.3: FAS confusion matrix related to the NPREL configuration in clean condition. The average precision is 98.13%, the average recall 98.05%, and the average  $F_1$ -Measure 98.06%.

	Doll	Bag	Ball	Basket	Book	Chair	Fork	$F_1$
Doll	100.00	0	0	0	0	0	0	100.00
Bag	0	97.73	0	0	2.27	0	0	97.73
Ball	0	0	100.00	0	0	0	0	100.00
Basket	0	0	0	95.45	2.27	2.27	0	97.67
Book	0	2.27	0	0	97.73	0	0	94.51
Chair	0	0	0	0	4.55	95.45	0	96.55
Fork	0	0	0	0	0	0	100.00	100.00
Precision	100.00	97.73	100.00	100.00	91.49	97.67	100.00	

the NPREL features, exceeds the one of the aerial microphone obtained with the standard MFCC pipeline by 8.76%. This value confirms that the higher SNR of the floor sensor signals actually results in better classification performance.

Regarding the features, the hypothesis that the pre-emphasis could be detrimental for the performance of the sensor is confirmed: indeed, the highest  $F_1$ -Measure has been obtained with the NOPRE configuration and exceeds the one of the standard MFCC pipeline by 1.32%. Differently, the introduction of the low-pass filter does not result in better performance respect to the NOPRE case.

### Results in multicondition

Figure 4.7 shows the results obtained in multicondition, i.e., when training and test sets both contain clean and noisy data. The results further confirm the superiority of the FAS respect to the aerial microphone, with the first reaching 90.82% using the NOPRE features and the latter reaching 85.28% using the standard MFCC pipeline. Regarding the features, Figure 4.7 confirms that removing the pre-emphasis indeed improves classification results, while introducing the low-pass filtering does not give further benefits.

#### 4.1.5 Remarks

The experimental results taken as a whole provide important insights on the system behavior and allow us to express possible future directions for its improvement. In particular, the experiments demonstrated the superiority of the floor acoustic sensor compared to the aerial microphone. The results in matched condition are notable, since the  $F_1$ -Measure is greater than 98% in clean condition and close to 90% in noisy condition. The experiment in matched condition is important to compare the performance of the two sensors, but it puts the classifier in a favourable scenario. The mismatched condition is closer to a real scenario, where the classifier is trained on a dataset whose characteristics differ

#### 4.2 Binary SVM based classifier for human fall detection

from testing ones. The floor sensor still achieves higher results compared to the aerial microphone, but respect to the matched condition they are considerably lower. This suggests that there is room for improvement both on the sensor side and on the algorithmic side.

Regarding the sensor, the insertion of isolating material in the enclosure would further reduce the impact of external interferences. On the algorithmic side, different low-level features could be employed instead of MFCCs. In particular, recalling the works on speech recognition systems, Power Normalized Cepstral Coefficients (PNCCs) [55] exhibited good performance in noisy conditions and could be considered also for fall classification. In addition, the SVM classifier here employed has not been designed to recognize a specific class. In the latter case, e.g., focusing on the human fall class, the problem can be tackled in two ways: as a two class problem, where one class is the class of interest and the other comprises “the rest of the world” that will be addressed in Section 4.2 or as a novelty detection problem, where the “novel” events are represented by the specific class occurrence that will be addressed in Section ???. In both cases, the classification task is simpler, since the number of classes to discriminate is reduced and the overall performance is expected to increase [35].

## 4.2 Binary SVM based classifier for human fall detection

The classification algorithm is based on the previous work. It employs both low-level features, i.e., MFCCs [56], and high-level features, i.e., Gaussian Mean Supervectors which are then used by a Support Vector Machine to distinguish falls from no-falls. Despite MFCCs were originally developed for speech and speaker recognition tasks, they have been successfully applied also for acoustic event classification [57] and fall detection [16]. Differently from the algorithm presented in the previous section, where the algorithm discriminated falls of general objects, here the focus is specifically on the classification of human falls. The classifier, thus, has been designed to discriminate between two classes: human falls and generic sound events. In order to assess the performance of the approach, the dataset described in Section 4.1.2 has been augmented with instances of everyday sounds (speech, footsteps, etc.), thus making the task more challenging. As a reference, results employing the original dataset (Section 4.1.2) are also reported.

## Chapter 4 Supervised Approach

### 4.2.1 Proposed approach

The classification algorithm is composed of two main parts. The first is the features extraction phase where we have extract the Mel Frequency Cepstral Coefficients from all audio files that comprise the dataset. For doing this, the feature extraction pipeline is the same used in Section 4.1.1. In particular, the signal is segmented in frames 16 ms long overlapped by 8 ms, the parameter  $\alpha$  of the pre-emphasis filter has been set to 0.97 and the number of filters which compose the filterbank has been set to 29. At the end, after the Discrete Cosine Transform, 13 statics coefficients are extracted that, together with their first and second derivatives, form the final feature vector of a signal. The classification phase is similar to that one adopted in Section 4.1.1: first it uses a mixture of gaussians (GMM), trained on a large corpus of audio events with the Expectation Maximization algorithm to model the acoustic space (Universal Background Model, UBM). Then, for each audio segment, the Maximum a Posteriori (MAP) algorithm is used to calculate the Gaussian Mean Supervector (GMS) from the MFCCs. In contrast with the previous work Section 4.1.1, where we used a multi-class approach, here we employ a binary SVM to discriminate the class “fall” from “rest” which allows to distinguish human falls from the other types of sounds. In addition, the class decision is usually performed by evaluating the sign of the SVM discriminative function, which ultimately consists in deciding whether in example belongs to a class by setting a threshold equal to zero. However, in a human fall classification task, it is important to minimize the probability of missing a fall event, i.e., false negatives. In order to push the system towards this direction, we decided to consider the entire value of the SVM discriminative function, and then to set an appropriate threshold in order to minimize the occurrence of false negatives.

### 4.2.2 Dataset

As can be seen in the Table 4.4, the dataset used for training and assess the proposed method is an enlarged version of the one used in Section 4.1. Moreover, in order to further stress the system, a 20 minutes long recording session in which 2 persons have produced everyday noises such as talking, walking, dragging chairs, and playing with the ball was used. Then the track obtained in this session has been divided in 665 sub-tracks. The lengths of these sub-tracks have been randomly generated with gaussian distribution. Mean value and standard deviation of this distribution have been calculated based on the lengths of the other files that form the dataset. In addition to the clean dataset, a noisy version has been created to assess the performance in noisy condition. The noisy dataset consists in a musical background recorded with both sensors and digitally added to the clean events.

#### 4.2 Binary SVM based classifier for human fall detection

Table 4.4: Data related to R0 room used in this work.

Classes	Nr. of occurrences
Basket	44
Fork	44
Ball	44
Book	44
Bag	44
Chair	44
Manikin Doll	44
<b>Backgrounds</b>	<b>Total length (s)</b>
Classic Music	882
Rock Music	616
human activities	665

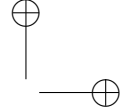
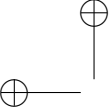
#### 4.2.3 Experiments

In this section, the experimental procedure is firstly discussed and then the algorithm performance is presented. In the experiments, the signals of the dataset described above have been downsampled to 8 kHz and the bit depth has been reduced to 16 bit. Both the choice of the sampling frequency and the choice of MFCCs are justified by the analysis performed in the Section 3.2.3, where it was shown that the signals recorded with the FAS have the majority of the energy concentrated at low frequencies (below 1 kHz). Indeed, the mel scale used in the feature extraction pipeline has a higher resolution at low frequencies, that allows to better describe the portion of the spectrum where the majority of the energy resides. In addition, the algorithm has been evaluated using two features extraction pipelines:

- the first is the same described in the Section 4.1.1 and will be denoted as STD;
- the second pipeline does not include the pre-emphasis filter and will be denoted with NOPRE.

The experiments have been conducted with a 4-fold cross-validation strategy and a three-way data split in three different operating conditions:

- matched, where the training, validation and test sets share the same acoustic condition, i.e., clean or noisy;
- mismatched, where the training set is composed of clean signals while the validation and test sets are composed of noisy signals;



## Chapter 4 Supervised Approach

- multicondition, where the training, validation and test sets contain both clean and noisy data. In this case the sets have been divided so that they contain 1/3 of clean data and 2/3 of noisy data.

The tests have been conducted also without using the signals of everyday noises, i.e., using the same dataset employed in Section 4.1.2. The performance is evaluated in terms of  $F_1$ -Measure per class and the values have then been averaged to obtain a single performance metric. To better describe the algorithm behavior, we have used the Detection Error Trade-off (DET) curve, as defined in [58]. This graph allows evaluating the false alarm probability when miss probability is equal to 0 (henceforward named as FPM0), which is particularly relevant in a fall classification task.

### 4.2.4 Results

#### Results in matched condition

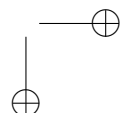
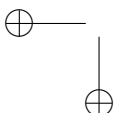
Figure 4.8 shows the results obtained in the matched condition case study using the enlarged version of the dataset. In Figure 4.8a, the FAS achieves higher  $F_1$ -Measures both in clean and noisy conditions. In the first case, the floor sensor exceeds the  $F_1$ -Measure of the aerial microphone obtained with the standard MFCC pipeline by 0.11%. In the noisy condition case study, the FAS with STD features achieves an  $F_1$ -Measure greater than 0.3% with respect to the aerial microphone with NOPRE features.

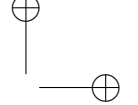
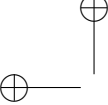
The DET curves are shown in Figure 4.8b. Note that the lines relative to the FAS in clean condition are both absent. This is because independently from the threshold, either the miss probability or the false alarm probability is 0 and the DET curves assume values towards minus infinite (in logarithmic scale). This means that the FPM0 are 0 for both these configurations, while the lower FPM0 for the aerial microphone in clean condition is 1.3%. Regarding the tests with noisy signals, the performance difference between the two sensors increases, since the FPM0 is equal to 2.2% with the FAS (NOPRE) and is equal to 12.5% with the aerial sensor (STD).

In order to facilitate the analysis, Table 4.5 summarises the results obtained with the dataset version used in Section 4.1.2, which does not comprise everyday noises. As it can be observed, with respect to the previous results, the performance decreases in all tests and for both the  $F_1$ -Measure and the FPM0, although the gap between the FAS and the aerial microphone increases.

#### Results in mismatched condition

The mismatched condition is the most difficult case for the classifier. As expected, the performance decrease for both sensors. Focusing on Figure 4.9a,





## 4.2 Binary SVM based classifier for human fall detection

Table 4.5: Fall classification performance in matched condition with the dataset excluding everyday noises.

		STD		NOPRE	
		$F_1$ -Measure	FPM0	$F_1$ -Measure	FPM0
Clean	Aerial	96.29	9.85	93.11	4.95
	FAS	98.81	0.00	100.00	0.00
Noisy	Aerial	97.22	43.00	96.92	73.00
	FAS	99.63	6.05	99.62	9.85

the best  $F_1$ -Measure is obtained with the NOPRE pipeline for both the FAS and aerial microphone, and is equal to 99.14% and 98.43% respectively. A consistent performance difference between the two sensors can be observed in Figure 4.9b, where the smallest FPM0 for the FAS, obtained with NOPRE, is around 13% while for the aerial one is 95%, this time obtained with STD.

The results of the mismatched experiments obtained with the dataset without everyday noises are reported in Table 4.7a. Regarding the  $F_1$ -Measure, a performance decrease can be observed compared to the results in Figure 4.9a. Differently, the aerial microphone FPM0 improves, but it is again below the FPM0 achieved by the FAS with NOPRE MFCCs (12.5%).

### Results in multicondition

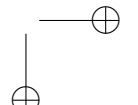
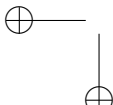
Figure 4.10 shows the results in the multicondition case. The FAS superiority is confirmed, since it achieves an  $F_1$ -Measure equal to 99.78% regardless the feature extraction pipeline, while the aerial sensor obtains an  $F_1$ -Measure equal to 99.19% with the STD pipeline.

Regarding the DET plot (Figure 4.10b), an FPM0 equal to 2.9% is achieved by the FAS, but differently from the previous cases, with the STD feature. The aerial microphone achieves an FPM0 equal to 9.8% with the NOPRE pipeline.

In the last table (Table 4.7b) are shown the result of the multicondition tests obtained by using the smaller dataset. Again there is an overall decrease for the  $F_1$ -Measure, greater for the aerial microphone, while the FAS exhibiting a FPM0 equal to 0% contrary to the increasing FPM0 for the aerial sensor.

#### 4.2.5 Remarks

In this section, a human fall classification system based on the previous work discussed in Section 4.1 has been described. The main sensor used in the FAS the sensor operates similarly to stethoscopes, with a microphone embedded in a resonant enclosure and a membrane in contact with the floor that captures the acoustic waves resulting from a fall. The performance of that sensor has



#### Chapter 4 Supervised Approach

Table 4.6: Fall classification performance in mismatched condition (a) and multicondition (b) with the dataset excluding everyday noises.  $F_1$  denotes the  $F_1$ -Measure.

		(a)			
%		STD		NOPRE	
		$F_1$	FPM0	$F_1$	FPM0
Aerial		96.20	87.50	95.44	76.00
FAS		97.80	34.50	98.11	12.50

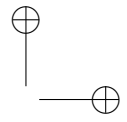
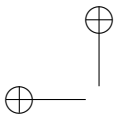
		(b)			
%		STD		NOPRE	
		$F_1$	FPM0	$F_1$	FPM0
Aerial		96.80	16.50	96.78	31.4
FAS		99.62	0.00	99.43	0.00

been compared with the one obtained by a standard aerial microphone. The classification algorithm extracts MFCC features from the signal acquired with the FAS, and then discriminates a fall from a generic event by using GMM supervectors and an SVM classifier. Differently from the works discussed in Section 4.1, here we specifically addressed the human fall classification task by designing the classifier to discriminate human falls from other events.

The performance of the system has been evaluated on a corpus containing recordings of several events: falls of a human mimicking doll, falls of common objects and everyday noises (speech, footsteps, etc.). In order to assess the performance of the solution in adverse acoustic conditions, a noisy version of the dataset has been created. The experiments have been performed in three operating conditions: matched, mismatched and multicondition, and the performance has been evaluated in terms of average  $F_1$ -Measure and false alarm probability when the miss probability is equal to 0. The superiority of the FAS resulted evident in all the addressed conditions, in particular with an  $F_1$ -Measure equal to 100% and an FP0 equal to 0% in clean matched conditions, and an  $F_1$ -Measure equal to 99.14% and an FP0 equal to 13% in noisy mismatched conditions.

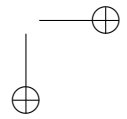
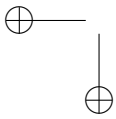
Moreover, by looking at the results obtained with the two different features pipeline, the FAS based solution always show robust performance and it is difficult to determine which represents the best choice. The increasing performance ( $F_1$ -Measure) obtained with the largest version of dataset, in truth, are due to the fact that signals corresponding to the everyday noises are extremely easy to classify being very different from a fall.

As future works, the datasets will be expanded in order to evaluate the system performance in case the falls occurs in a different room respect to the

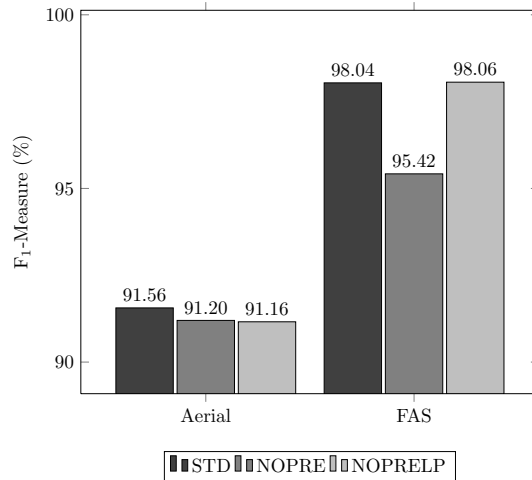


#### 4.2 Binary SVM based classifier for human fall detection

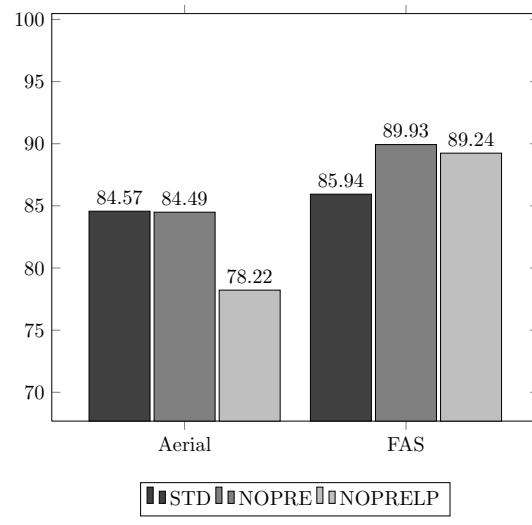
FAS one or in different scenario as falls occurs in presence of furniture or with a different paving. Both this aspect will be addressed in Section ???. In addition, the detection of the time boundaries of the fall event will be addressed and techniques originally developed for enhancing speech will be evaluated to increase the robustness to acoustic distortions [59, 60].



*Chapter 4 Supervised Approach*



(a)



(b)

Figure 4.5: Fall classification performance in matched condition with clean (a) and noisy signals (b).

#### 4.2 Binary SVM based classifier for human fall detection

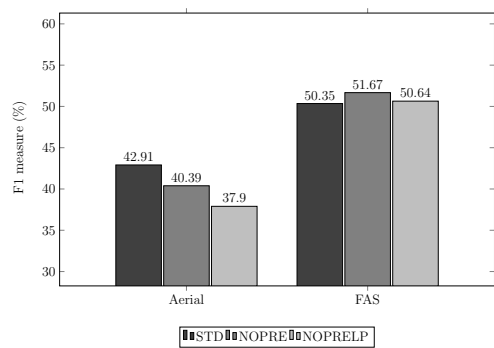


Figure 4.6: Fall classification performance in mismatched condition.

Chapter 4 Supervised Approach

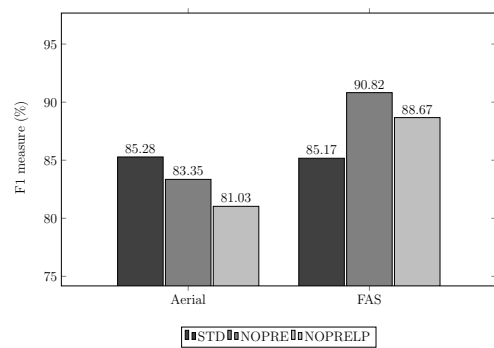
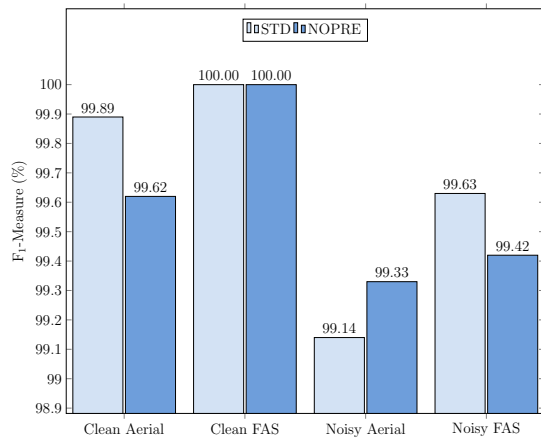
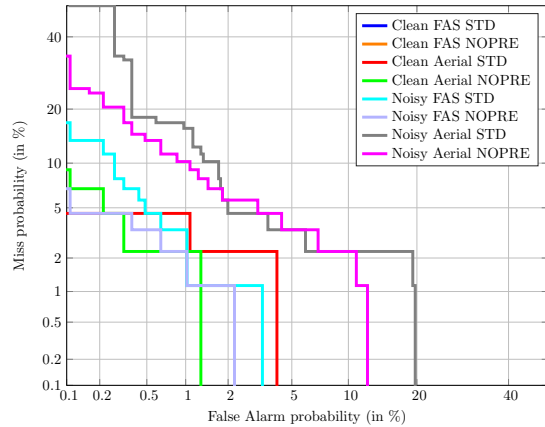


Figure 4.7: Fall classification performance in multicondition.

#### 4.2 Binary SVM based classifier for human fall detection



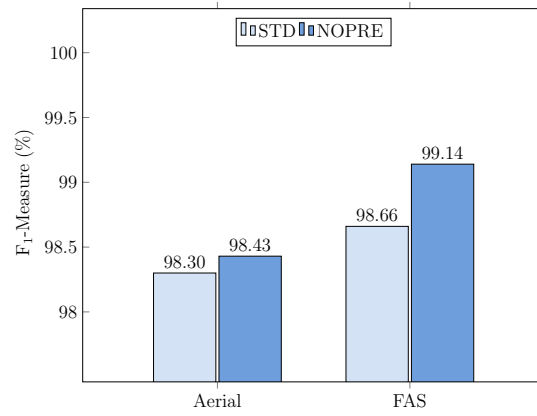
(a) F<sub>1</sub>-Measure histogram plot.



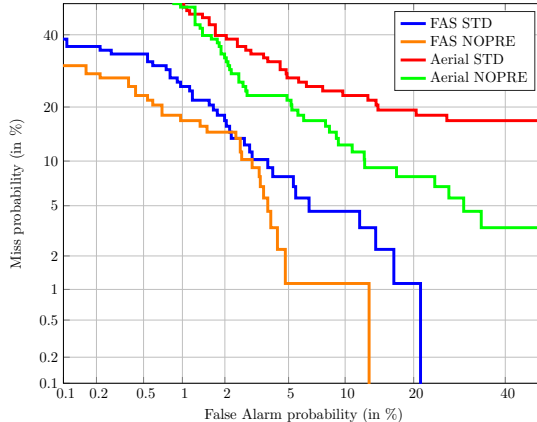
(b) Comparison of DET graphs.

Figure 4.8: Fall classification performance in matched condition with the dataset comprising everyday noises.

*Chapter 4 Supervised Approach*



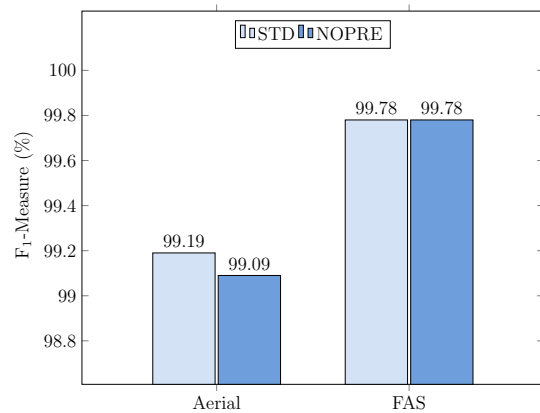
(a) F<sub>1</sub>-Measure histogram plot.



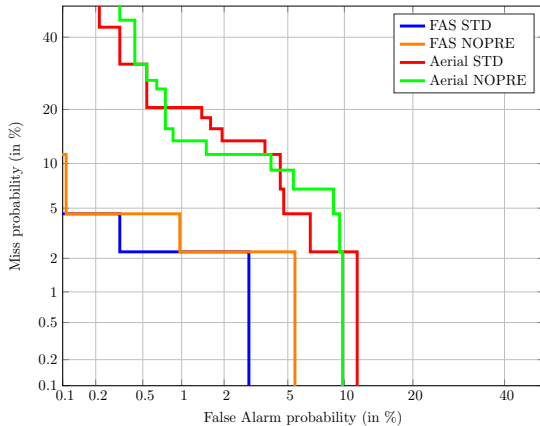
(b) Comparison of DET curves.

Figure 4.9: Fall classification performance in mismatched condition with the dataset comprising everyday noises.

#### 4.2 Binary SVM based classifier for human fall detection

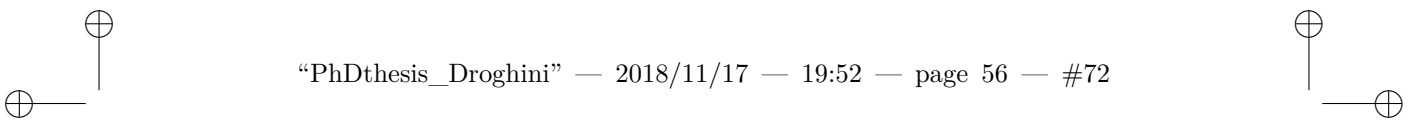


(a) F<sub>1</sub>-Measure histogram plot.



(b) Comparison of DET curves.

Figure 4.10: Fall classification performance in multicondition with the dataset comprising everyday noises.



“PhDthesis\_Droghini” — 2018/11/17 — 19:52 — page 56 — #72



# Chapter 5

## Unsupervised Approach

The problem with supervised approaches is that they require that each class of interest is represented in the training dataset. However, with real human falls the variability of the environmental conditions and of the subjects makes difficult or impossible to collect a sufficient number of examples that allow the algorithm to generalize well on unseen conditions [61]. Unsupervised approaches tackle the problem as a novelty detection task [62, 63], i.e., by learning a normality model from data not related to human falls.

da qui in poi si usa solo il FAS poerchè è stato appurato che è migliore dei microfoi aerei

### 5.1 Novelty detection algorithm for human fall detection based on One-Class Support Vector Machine

The approach proposed in this section is based on a One-Class Support Vector Machine (OCSVM) [37] to obtain an unsupervised framework for Fall Detection. The acoustic signals are captured by means the Floor Acoustic Sensor and then MFCCs and Gaussian Mean Supervectors (GMSs) are extracted by using the same methods described in Section 4.1.1: GMSs are higher level features computed by adapting the means of a Gaussian mixture model (GMM) with maximum a posteriori algorithm (MAP). In the training phase, a large set of audio data is used to model an Universal Background Model (UBM) composed of the GMM extracted by using Expectation Maximization (EM) algorithm [52]. Then, the GMS of each event is calculated by adapting the GMM with the MAP algorithm and concatenating the resulting GMM mean values. Abnormal acoustic events are discriminate from normal ones employing the OCSVM classifier.

## Chapter 5 Unsupervised Approach

Table 5.1: Composition of the dataset.

Class	Nr. of occurrences	Total length (s)
Basket	64	86
Fork	64	82
Ball	64	129
Book	64	63
Bag	64	57
Chair	96	157
Human Falls	44	76
Human Activity	665	1218
Music	776	1498

### 5.1.1 Dataset

The performance of the algorithm has been evaluated on a corpus containing sounds of human falls, falling objects, human activities, and music. In particular, from the dataset presented in Section 3.2, have been used the samples reported in Table 5.1.

Musical tracks and normal activities sounds have been divided in segments whose lengths have mean and standard deviation estimated from instances of fall events. In addition, they have been employed alone and to create noisy versions of human and object falls occurrences in order to assess the algorithm in presence of interferences.

In the experiments, signals have been downsampled to 8 kHz and the resolution has been reduced to 16 bit. As in the approach presented previously, the choice of the sampling frequency is motivated by the analysis performed in a previous work by the authors Section 3.2.3, where it was shown that the signals recorded with the FAS have the majority of the energy concentrated at frequencies below 1 kHz.

### 5.1.2 Experimental setup

The dataset described previously has been divided in one set for training the UBM and the OCSVM and three sets for evaluating the performance.

Training has been performed on the set shown in Table 5.2 composed of 947 occurrences (1773 s) of human activities, classical music and rock music. The assessment of the algorithm has been performed on the following datasets:

- Set 1 (Human fall and background sounds): this set comprises 44 examples of human fall sounds and 44 examples of human activity and music sounds (Table 5.3).

### 5.1 Novelty detection algorithm for human fall detection based on One-Class Support Vector Machine

Table 5.2: Composition of the training-set.

Class	Nr. of occurrences	Total length (s)
Human Activity	320	593
Music	627	1180
Total	947	1773

Table 5.3: Composition of “Set 1”.

Class	Nr. of occurrences
Human Falls	44
Human Activity	15
Music	29

- Set 2 (Human fall and object fall sounds): this set comprises 44 examples of human fall sounds and 44 examples of object fall sounds (Table 5.4).
- Set 3 (Human fall, object fall and background sounds): this set comprises 44 examples of human fall sounds, 22 examples of background sounds and 22 examples of object fall sounds (Table 5.5).

For each set, the data have been divided in four folds, each composed of 11 human falls and 11 non-falls. Then, one fold has been used for estimating the hyperparameters of the algorithm and three for calculating the performance. The final performance is calculated by using the cumulative true positives, false positives, and false negatives obtained by varying the test folds. The validation phase consisted in searching for the number of components of the UBM, the values of  $\nu$  and  $\gamma$  of the OCSVM. The values assumed by these variables are summarised in Table 5.6.

The proposed approach has been compared to the algorithm presented in [64] based on OCSVM. The same algorithm has also been employed in [19] with a multi-microphone acquisition setup and a source separation stage. As in [64], the audio signals are divided in windows of the same lengths, and the related MFCCs are used for training the OCSVM and for classification. In [64], 7 MFCCs were extracted from audio signals sampled at 20 kHz and the length of the window was set to 1 s. Here, the feature vectors are the same of the proposed approach, i.e., they are composed of the first 13 MFCCs and their first and second derivatives. The same window length of [64] cannot be employed here, since the dataset used in this paper comprises signals with lengths less than 1 s. Thus, the length of the window corresponds to the duration of the

## Chapter 5 Unsupervised Approach

Table 5.4: Composition of “Set 2”.

Class	Nr. of occurrences
Human Falls	44
Basket	7
Fork	7
Ball	8
Book	7
Bag	8
Chair	7

Table 5.5: Composition of “Set 3”.

Class	Nr. of occurrences
Human Falls	44
Basket	3
Fork	4
Ball	4
Book	3
Bag	4
Chair	4
Human Activity	8
Music	14

shortest event in the dataset, and it is equal to 576 ms (71 frames). Windows are overlapped by 50%, and, as in [64], an event is classified as fall if at least two consecutive frames are classified as novelty by the OCSVM. The same grid search procedure of the proposed approach has been adopted to search for the optimal values of  $\nu$  and  $\gamma$  of the OCSVM.

The performance has been evaluated in terms of F<sub>1</sub>-Measure calculated as:

$$F_1\text{-Measure} = \frac{2 \cdot tp}{2 \cdot tp + fn + fp}, \quad (5.1)$$

where  $tp$  is the number of correctly classified falls,  $fn$  is the number of falls misclassified as non-falls, and  $fp$  is the number of non-falls misclassified as falls.

### 5.1 Novelty detection algorithm for human fall detection based on One-Class Support Vector Machine

Table 5.6: Hyperparameters of the algorithm and search space explored in the validation phase.

Stage	Hyperparameter	Range
UBM	$J$	1, 2, 4, ..., 64
OCSVM	$\nu$	0.1, 02, ..., 1.0
	$\gamma$	$2^{-15}, 2^{-13}, \dots, 2^3$

#### 5.1.3 Results

Figure 5.1 shows the results in clean conditions obtained with the proposed method named “OCSVM” and the comparative method proposed in [64] denoted as “Popescu (2009)”. Observing the figure, it is evident that in all the three cases the OCSVM approach is able to improve the performance with respect to “Popescu (2009)” [64]. In particular, in “Set 1”, that comprises human falls, human activities and music, the performance improves by 16.73% with respect to “Popescu (2009)”. This case can be considered as the least challenging of the three, since non-falls events are considerably different from falls ones. Conversely, “Set 2” comprises both human falls and object falls, thus it includes abnormal events whose pattern is similar to the one of human falls. Indeed, the performance with respect to “Set 1” is 17.91% lower, mostly due the increased false positives rate that goes from 13.64% to 50.76%. Regarding “Popescu (2009)” [64], the  $F_1$ -Measure is below both OCSVM and the proposed approach, however it is less affected by the presence of object falls, since the  $F_1$ -Measure decreases only by 0.64%. “Set 3” comprises human falls, human activities, music and object falls and represents the most realistic test condition of the three. The results obtained by using the OCSVM classifier alone is 82.25%. As expected, this result is lower than “Set 1”, since object falls are also present, and higher than “Set 2”, since human activities and music segments are easier to discriminate. Differently, the approach by Popescu and Mahnot [64] degrades by 5.25% with respect to “Set 1”, and by 4.61% with respect to “Set 2”, demonstrating that it is less robust to the concurrent presence of object falls and daily human activities sounds.

Figure 5.2 shows the results obtained for the three cases in noisy conditions. As expected, the performance decreases in all the two evaluated methods. In “Set 1”, the performance decrease is modest (2.32% for the OCSVM and 1.44% for “Popescu (2009)”), demonstrating that the OCSVM is able to effectively reject non-fall events corrupted by music interference. In “Set 2”, the presence object falls corrupted by music significantly decreases the performance of the OCSVM, reducing the  $F_1$ -Measure by 12.74% with respect to the clean “Set 2”. The method by Popescu and Mahnot [64] achieves the highest  $F_1$ -Measure in this case, confirming the good capabilities of rejecting dropping objects sound

## Chapter 5 Unsupervised Approach

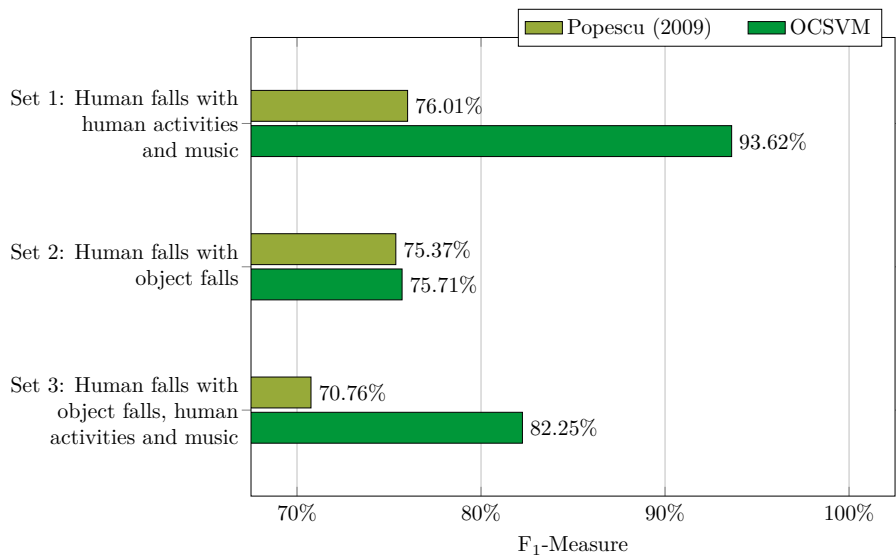


Figure 5.1: Results in *clean* conditions for the three test cases. “Set 1” comprises human falls, human activities and music. “Set 2” comprises human falls and object falls. “Set 3” comprises human falls, object falls, human activities, and music.

events observed in clean conditions. In “Set 3”, the proposed approach improves the performance by 3.91% with respect to “Popescu (2009)”, confirming that it is able to achieve the highest performance in the most realistic scenario of the three.

## 5.2 End-To-End Unsupervised Approach employing Convolutional Neural Network Autoencoders for Human Fall Detection

In recent years, thanks to the success of deep learning methods have become increasingly popular the feature learning approaches that independently transform the raw data inputs to a representation that can be exploited in machine learning tasks, minimizing the need of prior knowledge of application domain. Furthermore, such approaches are often able to generalize well real-world data compared to traditional hand-crafted features [65], resulting in an increase in performance of classification or regression tasks. The end-to-end learning is a particular example of feature learning, where the entire stack, connecting the input to the desired output, is learned from data [66]. As in feature learning, only the tuning of the model hyperparameters requires some expertise, but

## 5.2 End-To-End Unsupervised Approach employing Convolutional Neural Network Autoencoders for Human Fall Detection

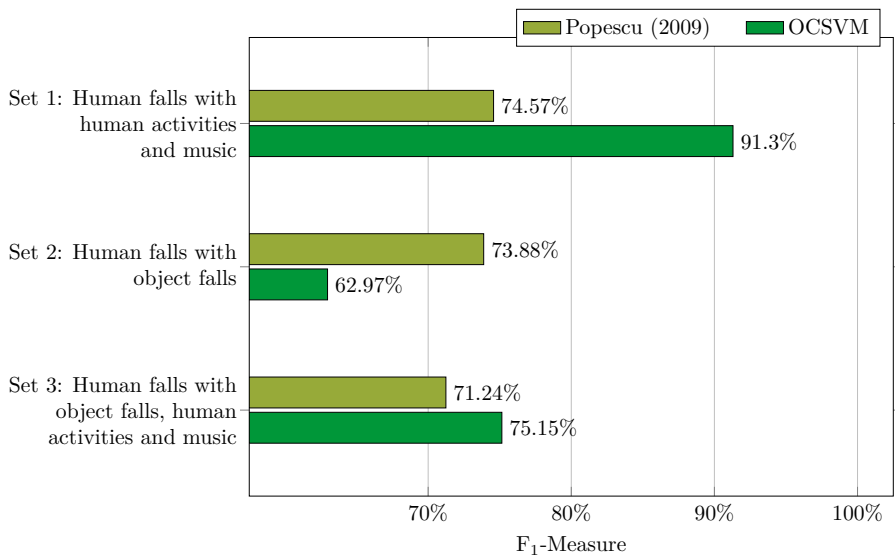


Figure 5.2: Results in noisy conditions for the three test cases. “Set 1” comprises human falls, human activities and music. “Set 2” comprises human falls and object falls. “Set 3” comprises human falls, object falls, human activities, and music.

even that process can be automated [67].

In this section, an end-to-end acoustic fall detection approach is presented. A deep convolutional neural network autoencoder is trained with the signals, gathered by the Floor Acoustic Sensor (Section 3.1), corresponding to sounds that commonly occurring in a home (e.g., voices, footsteps, music, etc.). Since the sound produced by a human fall should be considerably different from the ones used for the training, it will be recognized as “novelty” by the network and classify as Fall. The performance of the algorithm has been evaluated on a subset of the dataset described in Section 3.2, which contains human fall events simulated by employing the “Rescue Randy” human mimicking doll [68, 16, 27] and sounds related to common human activities. Dieleman *et al.* [69] address the content-based music information retrieval tasks, investigating whether it is possible to apply end-to-end feature learning directly to raw audio signals instead than on a spectrogram representation of data. Up to the authors’ knowledge, the end-to-end strategy has never been applied to a unsupervised fall detection approach with acoustic sensors. However, many works in other research fields can be found in literature. Their convolutional neural networks trained on raw audio signals do not outperform a spectrogram-based approach in the automatic tagging task but are able to autonomously discover frequency decompositions from raw audio, as well as phase and translation-invariant fea-

## Chapter 5 Unsupervised Approach

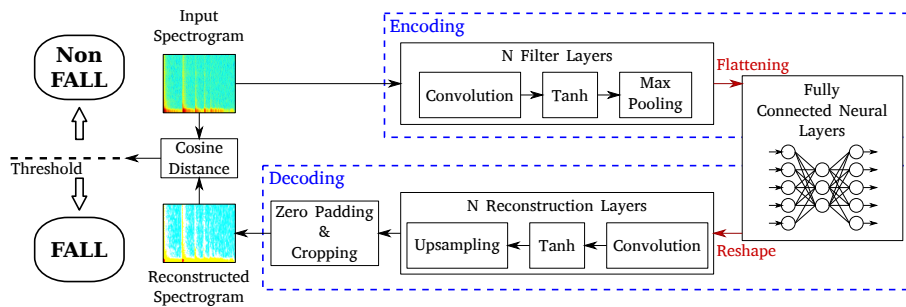


Figure 5.3: The proposed approach scheme.

ture representations. The contribution is a novel fall detection method which exploits the end-to-end approach, resulting in a reduction of the engineering effort needed to design the system, with respect to those method that used features extracted from input signals. Is also shown that it can achieve good performance, higher than two state-of-the-art systems chosen for a comparison.

### 5.3 Proposed Approach

In the state of the art the majority of fall detection systems are logically designed as a cascade of elements which perform some sub-task (e.g. feature extraction, modeling, classification, ecc.). Each task is independently developed and generally requires the tuning of a number of hyperparameters using an experimental procedure and some a prior knowledge about the domain of the problem.

The proposed approach, showed in Figure 5.3, is designed according to the end-to-end paradigm and then, the entire stack, connecting the input to the desired output, is learned from data. End-to-End is a feature learning strategy that, in presence of sufficient training data, may result in better performance than systems based on handcrafted features, since the training procedure automatically select the salient information. Therefore, if were possible to analyze the feature learned by the network with end-2-end strategy, there should be clues about what kind of information is important for a specific task.

The system core is a deep convolutional neural network autoencoder. Some exhaustive discussion about this type of network can be easily found in literature [70, 71, 72]. The network input consists of the normalized log-power spectrograms of the signals calculated with a STFT on windows of 32 ms and overlapped by 50%. Due to the presence of fully-connect neural layers, the input dimensions must be fixed. After having identified the widest spectrogram extracted from the dataset, the other ones have been extended with some AWGN frames added at the end. Each input consist in a  $f \times t$  matrix, where

## 5.4 Experiments

$f$  are the positive points of discrete Fourier transform and  $t$  are the number of windows considered in time. The output of the autoencoder are the reconstructed spectrograms. To classify an event, a distance measurement between input and output must be made with some heuristic. If the distance exceeds a certain threshold, automatically defined by the algorithm during the training phase, the system label the output as "Fall" or as "Non Fall" otherwise. In this work the cosine distance has been used:

$$D_C(v, u) = 1 - \frac{u \cdot v}{\|u\| \|v\|} = 1 - \frac{\sum_{k=1}^n u(k)v(k)}{\sqrt{\sum_{k=1}^n u(k)^2} \sqrt{\sum_{k=1}^n v(k)^2}} \quad (5.2)$$

where  $u$  and  $v$  are the vectors obtained flattening the input and the output spectrograms and  $n$  are the length of these vectors. According to the cosine definition, the value of the distance always has a value between  $-1$  and  $+1$ , where  $+1$  indicates two equal vectors while  $-1$  indicates two opposite vectors. The added AWGN part of the spectrums was not considered to calculate the distance. The choice of this heuristic allowed to make distance measurements independent of the size of the initial spectrum. The structure of the autoencoder is not defined a priori, but it is chosen through a phase of cross-validation during which the network parameters are varied with a random search strategy.

## 5.4 Experiments

In this section are described the composition of the dataset used in this work and the experimental set-up.

### 5.4.1 Dataset

The instances used in this approach are summarized in table Table 5.7. It is composed of two type of sounds: the first, namely novelty, comprises several human fall sounds that have been simulated by means of a human-mimicking doll employed in water rescues. The doll has been dropped from upright position and from a chair, both forward and backward. The drops have been then repeated at three distances from the FAS, i.e., 2, 4 and 6 m, for a total of 44 events, all included in the “Human fall” class. The second type, i.e., the background, comprises sounds of normal activities (voices, footsteps, etc.) for a total of 1218 s, and three musical tracks<sup>123</sup>, for a total of 1498 s, played from a loudspeaker and acquired back with the FAS. In addition, the signals of the second type have been employed alone and to create noisy versions of human

<sup>1</sup>W. A. Mozart, “Piano trio in C major”

<sup>2</sup>Led Zeppelin, “Dazed and confused”

<sup>3</sup>Led Zeppelin, “When the levee breaks”

## Chapter 5 Unsupervised Approach

Table 5.7: Composition of the dataset.

Class	Nr. of occurrences	Total length (s)
Human Falls	44	76
Human Activity	665	1218
Music	776	1498

falls occurrences in order to assess the algorithm in presence of interferences. The signals have been acquired with a sampling rate equal to 44.1 kHz and 32 bit depth. Based on previous experience in using the FAS, in order to exploit the acoustic characteristics of the sensor, signals have been downsampled to 8 kHz and the resolution has been reduced to 16 bit.

### 5.4.2 Experimental Setup

Since in this work a novelty approach is presented, the dataset has been divided in two groups: the former composed only of background sounds (i.e. human activity sounds and musical background) used for the training; the latter composed of both background sound and novelty sounds, i.e., the human falls, used in development and test phase. In order to assess the classification accuracy in noisy conditions, a second version of human fall sounds were created in which a musical background was recorded and then digitally added to the fall events.

The input spectrograms of the audio signals has been calculated with a fft point number of 256 and a windows size of 256 samples (32 ms at sample rate of 8000 kHz). The longest spectrogram present in the dataset is composed of 197 frame. Therefore the resulting input matrix dimension  $f \times t$  is  $129 \times 197$ . The optimization of the experiment hyper-parameters has been carried out using the random-search technique. Table 5.8 shows the parameters used in the random-search, and their ranges. The parameters of the network architecture are related only to the encoding part of autoencoder since the decoding part is its mirrored version. Instead other parameters, described below, have been set to the same value for all experiments. The activation function for each layer, whether they are convolutional or fully connected, have been set to *tanh*. “Adam” [73] has been used as optimization algorithm for the traing phase. The loss function used was *mlse*. The initialization algorithm for the weight of the autoencoder was Glorot Uniform [74]. The number of epoch has been set to 1000, while the patience, that is the number of epoch without an Auc improvement on a devset to wait before stopping the training phase, has been set to 40.

In order to implements a 4 fold cross-validation, the signals not being part of

#### 5.4 Experiments

Table 5.8: Hyper-parameters optimized in the random-search phase, and their range.

Parameter	Range	Distribution	Parameter	Range	Distribution
Cnn layer Nr.	[1-3]	uniform	Batch size	[10%-25%]	log-uniform
Kernel shape	[3x3-8x8]	uniform	Max pool shape	[1x1-5x5]	uniform
Kernel Nr.	[4-64]	log-uniform	Max Pool	All <sup>4</sup> -Only end <sup>5</sup>	uniform
MLP layers Nr.	[1-3]	uniform	Dropout	[Yes-No]	uniform
MLP layers dim.	[128-4096]	log-unifom	Drop rate	[0.5-0.6]	normal
Stride	[1x1-3x3]	uniform	Learning rate	[10 <sup>-4</sup> -10 <sup>-2</sup> ]	log-unifom

Table 5.9: Best hyper-parameters find in random-search phase for *clean* and *noisy* condition

Parameter	Clean				Noisy			
	Fold1	Fold2	Fold3	Fold4	Fold1	Fold2	Fold3	Fold4
Cnn layer Nr.	3	3	3	2	3	3	3	3
Kernel shape	8x8	7x7	5x5	8x8	8x8	7x7	8x8	8x8
Kernel Nr.	[16,16,8]	[32,16,16]	[8,8,8]	[32,16]	[32,32,8]	[32,32,8]	[32,32,32]	[8,8,8]
Max Pool Position	only end	only end	all	all	only end	only end	all	only end
Max pool shape	5x5	3x3	5x5	4x4	3x3	5x5	5x5	3x3
Stride	3x3	3x3	1x1	3x3	3x3	3x3	1x1	3x3
MLP layers Nr.	2	1	1	1	2	2	1	3
MLP layers dim.	[16,231]	96	32	32	[48,153]	[16,2084]	128	[48,1952,1952]
Learning rate( $\times 10^{-4}$ )	4.89	4.08	15.09	15.44	1.56	4.46	1.01	1.00
Batch size	11.26%	10.81%	13.59%	21.10%	20.06%	12.55%	13.51%	13.13%
Drop rate	0.64	0.57	0.53	0.55	0.58	0.53	0.55	0.59

training-set have been divided in four folds, each composed of 11 human falls and 11 non-falls signals. Then, one fold has been used as validation-set and the remaining three for calculating the performance in test phase. In cross-validation phase the scores have been evaluated in term of AUC. Here also the optimal thresholds have been infer by searching points on ROC curves closest to the (0, 1):  $d_{min} = \sqrt{(1 - fpr)^2 + (1 - tpr)^2}$ . At the end the final performance has been evaluated in term of *F<sub>1</sub> – Measure* by mediating the results obtained on individual folds.

Since this approach share the same train-set (Table 5.2) and test-set (Section 5.3) that has been used in Section 5.1 for both the clean and noisy conditions, the results scored here were compared with those obtained showed in Figure 5.1 and related to Set 1.

#### 5.4.3 Results

The results for both clean and noisy are reported in Figure 5.4. The comparative algorithms are denoted with “Popescu (2009)” and “OCSVM” respectively, while the proposed approach is named “Autoencoder”. It is immediately clear that the proposed approach outperforms the other in both conditions. In fact, in clean condition, it gains about 1% compared to “OCSVM” and about 18.6%

<sup>4</sup>After each Conv. layer

<sup>5</sup>At the end of cnn part

## Chapter 5 Unsupervised Approach

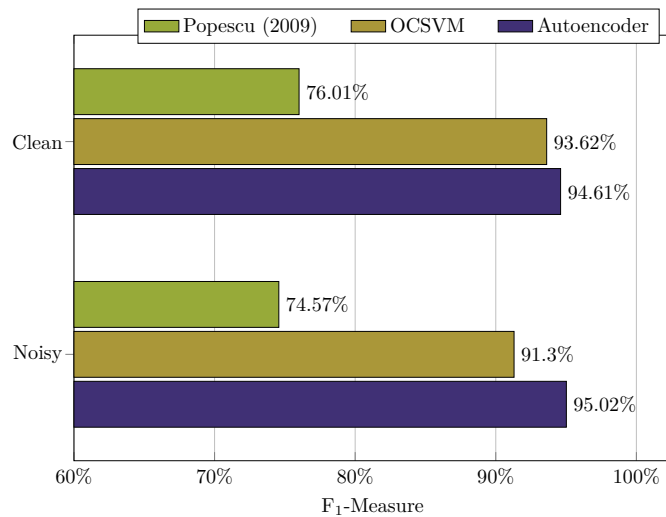


Figure 5.4: Results in *clean* and *noisy* conditions for the three test cases.

compared to “Popescu (2009)”. Moreover the proposed algorithm results to be very robust in noisy condition, whereas both other cases get worse a bit. In particular the performance improves by 3.72% with respect to “OCSVM” and by 20.45% with respect to “Popescu (2009)”. Clearly the end-to-end method seems insensitive with respect to the corrupted human fall signals when the novelty sounds are dissimilar respect to normality model learned from the background sounds. In Table 5.9 are reported the hyperparameters that have led to the results discussed above.

Furthermore other experiments were made up with a manual tuning of parameters. Particularly have been investigated deeper architectures composed up to 5 convolutional layer. We found that increasing the depth on cnn part (5 layers) with a different kernel number for each layers of [32,32,16,16,8] and a kernel dimension for all layers of 4x4, a max pooling after only the first three convolutional layer of 2x2 and two MLP layer of 1024 and 512, leads to considerable improvements. In effect the final  $F_1 - Measure$  rise up to 95,42% in both clean and noisy condition.

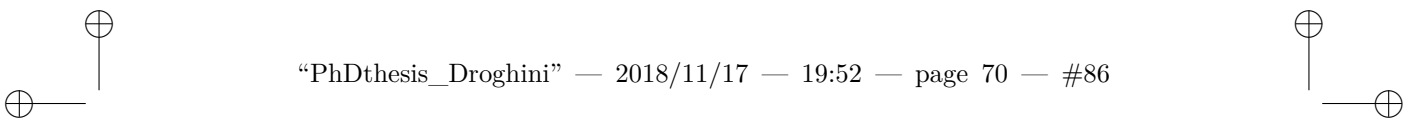
### 5.4.4 Remarks

The methods presented is an end-to-end approach composed by a deep-convolutional autoencoder with a downstream threshold classifier, that is a purely unsupervised approach to acoustic fall detection. Our method exploits the reconstruction error of the autoencoder. When a sound that the network has never seen in training phase occurs, the reconstruction error raise up allowing the recognition

#### 5.4 Experiments

of novelty. The algorithm has been trained with a large corpus of background signals, i.e, human activity noise and music, and evaluated with human-fall sound and other instances of background sounds. It has been evaluated in two different condition: the first with a clean version of human fall sounds and the second with corrupted version of the same. The results showed that the proposed solution leads to an average improvement about 20% with respect to the [64] and about 2.3% towards the OCSVM based approach.

In future works this approach will be assessed in a more realistic scenario including, in the test phase, others sound topologies such as falls of different objects, street sounds, etc., that could compromise the classification. In fact those sounds are much more similar to the human falls and could lead to a worse performance. In addition, having regard the results obtained with a manual tuning of parameters, deeper network architectures in combination with Recurrent Neural Network will be thoroughly investigated.



“PhDthesis\_Droghini” — 2018/11/17 — 19:52 — page 70 — #86



# Chapter 6

## Semi-Unsupervised Approach

Unsupervised methods, consider a human fall as an event that deviate from normality and they are based on one-class classifiers. The main advantage of an unsupervised methods for fall detection is that it can work without knowing any examples related to the class of interest, i.e. the human fall. As aforementioned, this should be the perfect way to go in an application like this, where what we are interested in is very difficult to retrieve or we only have very few data available, but the principal weakness of an unsupervised system is that certain events deviate from normality as the human fall (e.g., the fall of an object), thus they may produce false alarms. In this Chapter, two types of methods are described: in Section 6.1 a OCSVM user-aided method is exposed, while Section 6.2 present an approach based on Siamese neural network for one-shot learning, both of them assessed with samples related to R0 room of the employed dataset Section 3.2. An extension of the Siamese approach is presented in Section 6.2 where the entire dataset presented in Section 3.2 has been used.

### 6.1 A Combined One-Class SVM and Template Matching Approach for User-Aided Human Fall Detection

The approach proposed here, is the extension of the one presented in Section 5.1 thus, consists of a combined One-Class Support Vector Machine (OCSVM) based method and template-matching classifier that operate in cascade. The template-matching classifier operates in a user-aided supervised manner and it is employed to reduce such errors by using a set of templates that represent these events. Templates are identified by the user that marks the occurrence of a false positive instead of a true human fall event. As shown in the previous section, “unsupervised methods” are able to overcome the need of manual tuning of “analytical methods” and the necessity of a large labelled dataset of “supervised methods”. In “unsupervised methods”, falls are discriminated from

## Chapter 6 Semi-Unsupervised Approach

non-falls based on a model of “normality” constructed from a large amount of non-fall events. However, certain events differ from the “normality” as human falls, and they may induce the classifier to produce false alarms. As an example, Figure 6.1a and Figure 6.1b show respectively the waveform and the spectrogram of a segment of “normal” human activity (footsteps and speech) Figure 6.1c and Figure 6.1d show the waveform and the spectrogram of a segment of human fall, and Figure 6.1e and Figure 6.1f the waveform and the spectrogram of a book fall. The figures show clearly that both falls signals differ significantly from the human activity one, thus a classifier may be induced to consider the fall of a book as the fall of a person.

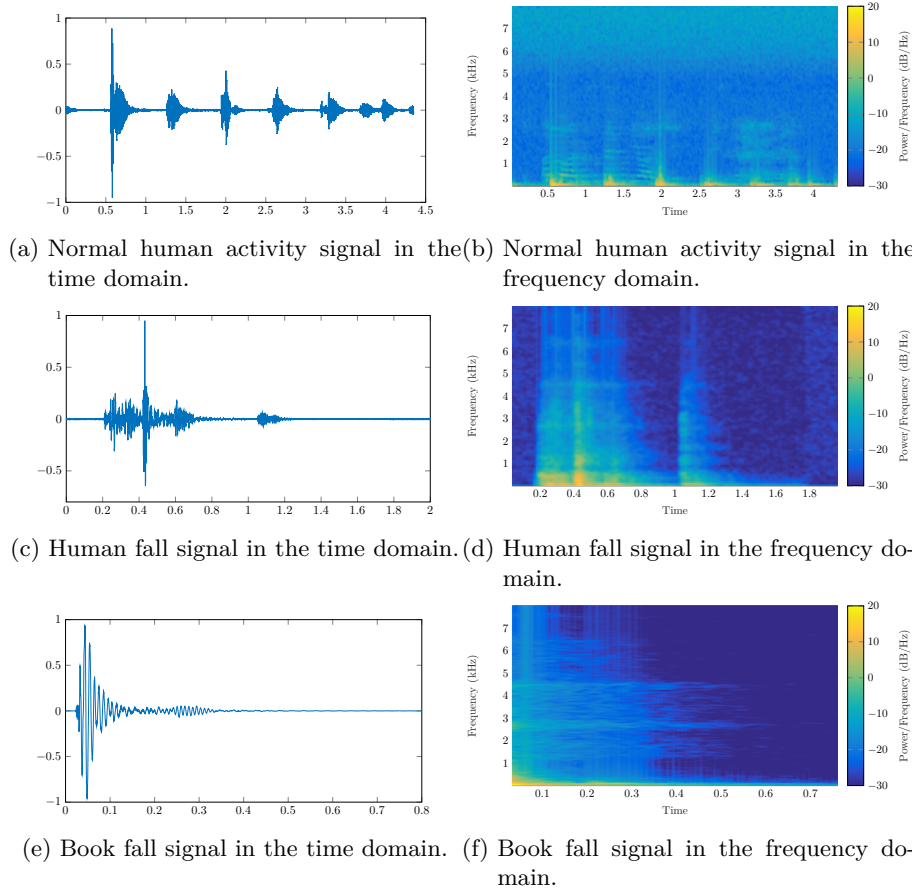


Figure 6.1: Time domain (on the left) and frequency domain (on the right) representation of a normal human activity signal (a-b), human fall signal (c-d), and book fall signal (e-f).

The algorithm proposed in this paper reduces the problem by employing a multi-stage classification approach that combines a one-class classifier based on

## 6.1 A Combined One-Class SVM and Template Matching Approach for User-Aided Human Fall Detection

OCSVM with a template-matching stage. The OCSVM is trained unsupervisedly on a large corpus containing sounds that represent the “normality”. On the contrary, the template-matching stage employs a set of templates represented by a small number of feature vectors marked as false alarm by the user. Thus, robustness against possible false alarms is achieved by using only few examples of false positive classes without the need of multiple sensors. An additional advantage with respect to the state of the art is that the proposed approach is able to evolve and improve after its initial training, since the template set can be augmented as non-falls events are detected.

### 6.1.1 Proposed approach

The proposed approach is composed of three stages Figure 6.2: the first (“Feature Extraction”) extracts MFCCs from the input audio signal and then GMSs to describe the entire audio segment. The second stage (“Abnormal Event Detection”) consists of a One-Class SVM classifier that discriminates between normal and abnormal sounds. Up to the authors’ knowledge, OCSVM together with GMSs have never been jointly used for acoustic fall detection. The third stage represents the innovative contribution of this paper for reducing false alarms in unsupervised approaches: it consists of a “Template-Matching” block that refines the output of the OCSVM and classifies the input data as fall or non-fall. The OCSVM is trained unsupervisedly on a large dataset of everyday sounds with the objective of discriminating normal from abnormal sounds. As aforementioned, the basic assumption is that the acoustic events related to human falls are “rare” respect to sounds normally occurring inside a home. The template-matching stage, on the other side, requires a set of “template” instances that represent rare events that can be confused with a fall. Referring to Figure 6.2, the “Template-Matching” stage is composed of a set of “Templates”, a block that calculates the distance between the input GMS and the templates (“Euclidean Distance Calculation”), and a “Decision” block that decides whether the event is a fall or a non-fall by evaluating the magnitude of the distance. The rationale here is that certain acoustic events are as abnormal as falls and confuse the OCSVM: the template-matching stage reduces false positives by using a set of examples related to the most confusing classes. In this work, the algorithm is “user-aided”, i.e., templates are indicated by the user each time the OCSVM produces a false positive. This is shown in Figure 6.2 with the person silhouette near the block that decides whether a detected fall is a false positive or not (“False Positive?”). In general, however, it is possible to create the templates set a-priori by recording several instances of possible false alarms events. Although rare, false alarm events (e.g., falls of objects) are certainly easier to reproduce in laboratory respect to human falls.

## Chapter 6 Semi-Unsupervised Approach

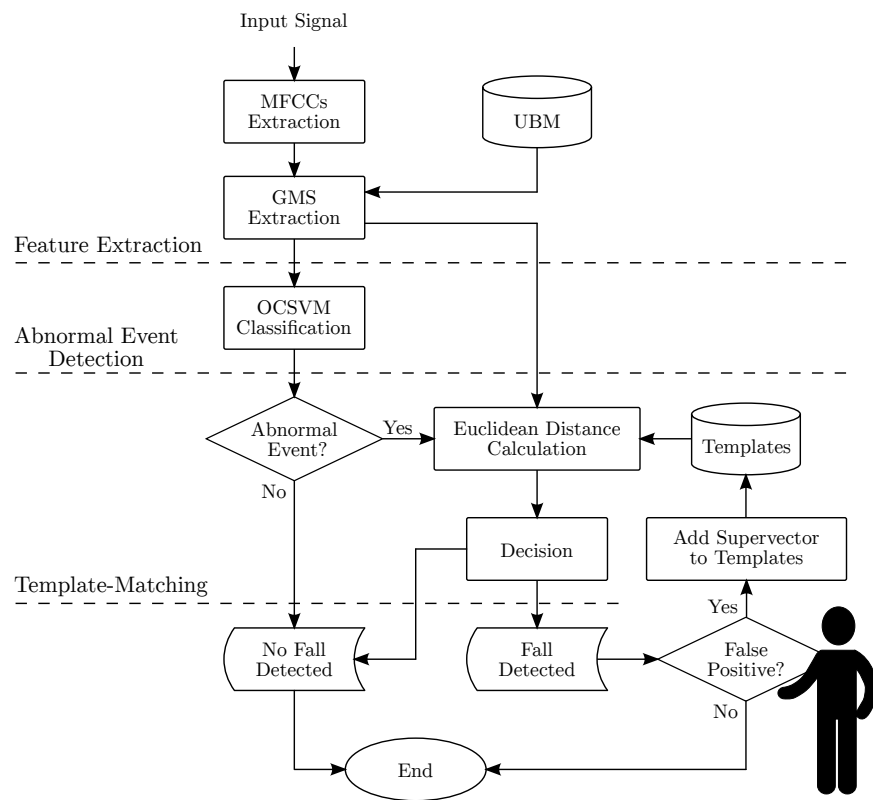


Figure 6.2: The block scheme of the proposed approach.

The remainder of this section describes the overall approach in details, starting from the acoustic sensor employed for capturing falls sounds, the feature extraction stage, and the combined OCSVM/template-matching stages.

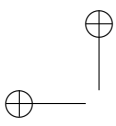
### 6.1.2 Dataset

The dataset employed in this method is reported in Table 5.2 of a previous section

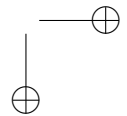
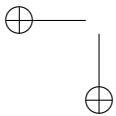
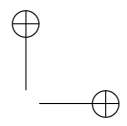
6.2 Few-shot Siamese Neural Networks employing Audio features for Human-Fall Detection

## 6.2 Few-shot Siamese Neural Networks employing Audio features for Human-Fall Detection

## 6.3 Audio Metric Learning by using Siamese Autoencoders for One-Shot Human Fall Detection

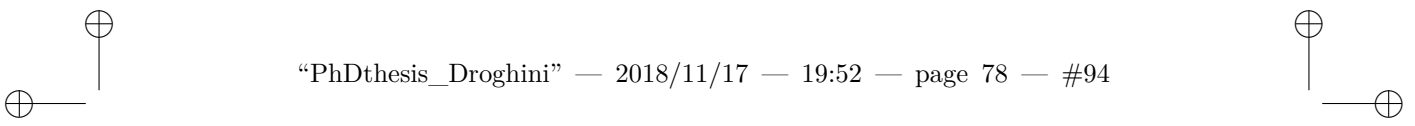


“PhDthesis\_Droghini” — 2018/11/17 — 19:52 — page 76 — #92



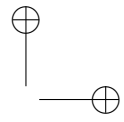
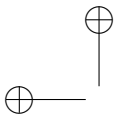
# Chapter 7

## Other contributions



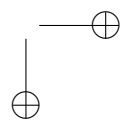
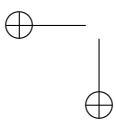
“PhDthesis\_Droghini” — 2018/11/17 — 19:52 — page 78 — #94

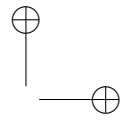
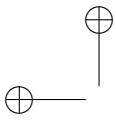




## List of Publications

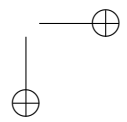
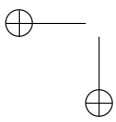
- [1] E. Principi, D. Droghini, S. Squartini, P. Olivetti, and F. Piazza, “Acoustic cues from the floor: a new approach for fall classification,” *Expert Systems with Applications*, pp. 51–60. vol. 60. Elsevier, 2016.
- [2] D. Droghini, E. Principi, S. Squartini, P. Olivetti, and F. Piazza, “Human Fall Detection by Using an Innovative Floor Acoustic Sensor,” *Proc. of WIRN*, Vietri sul Mare, Italy. May, 18-20, 2016.
- [3] E. Principi, D. Droghini, S. Squartini, P. Olivetti, and F. Piazza, “A Combined One-Class SVM and Template Matching Approach for User-Aided Human Fall Detection by Means of Floor Acoustic Features,” *Computational Intelligence and Neuroscience*, Hindawi, 2017.
- [4] D. Droghini, D. Ferretti, E. Principi, S. Squartini, and F. Piazza, “An End-To-End Unsupervised Approach employing Convolutional Neural Network Autoencoders for Human Fall Detection,” *Proc. of WIRN*, Vietri sul Mare, Italy. June, 14-16, 2017.
- [5] L. Gabrielli, C. E. Cella, F. Vesperini, D. Droghini, E. Principi, and S. Squartini, “Deep learning for timbre modification and transfer: An evaluation study,” *Proc. of 144th AES*, Milan, Italy, 24-26 May 2018, Audio Engineering Society.
- [6] F. Vesperini, D. Droghini, E. Principi, L. Gabrielli, and S. Squartini, “Hierarchic ConvNets framework for rare sound event detection,” *Proc. of EUSIPCO*. IEEE, Sept. 3-7 2018.
- [7] D. Droghini, F. Vesperini, E. Principi, S. Squartini, and F. Piazza, “Few-shot siamese neural networks employing audio features for human-fall detection,” *Proc. of The International Conference on Pattern Recognition and Artificial Intelligence*, Union, NJ, USA, Aug. 15-17 2018.
- [8] E. Principi, D. Droghini, S. Squartini, P. Olivetti, and F. Piazza, “A Combined One-Class SVM and Template Matching Approach for User-Aided Human Fall Detection by Means of Floor Acoustic Features,” *Engineering Applications of Artificial Intelligence*, Elsevier, 2018. Submitted.





**Others:**

- [1] F. Vesperini, D. Droghini, D. Ferretti, E. Principi, L. Gabrielli, S. Squartini, and F. Piazza, “A hierachic multi-scaled approach for rare sound event detection,” Ancona, Italy, 2017, DCASE Tech. Report. Copyright-free.
- [2] L. Gabrielli, F. Vesperini, D. Droghini, and S. Squartini, “Rima Glottidis: Experimenting generative raw audio synthesis for a sound installation,” *XXII Colloquium of Musical Informatics*, Udine, Italy, 20-23 Nov. 2018.



## Bibliography

- [1] “Eurostat statistic explained: Fertility statistics,” March 2016.
- [2] G. Carone and D. Costello, “Can europe afford to grow old?,” *Finance and Development*, vol. 43, no. 3, pp. 28–31, 2006.
- [3] P. Dawadi, D. Cook, and M. Schmitter-Edgecombe, “Automated cognitive health assessment from smart home-based behavior data,” *IEEE Journal of Biomedical and Health Informatics*, vol. 20, no. 4, pp. 1188–1194, 2016.
- [4] E. Principi, S. Squartini, R. Bonfigli, G. Ferroni, and F. Piazza, “An integrated system for voice command recognition and emergency detection based on audio signals,” *Expert Systems with Applications*, vol. 42, no. 13, pp. 5668–5683, 2015.
- [5] M. Mubashir, L. Shao, and L. Seed, “A survey on fall detection: Principles and approaches,” *Neurocomputing*, vol. 100, pp. 144–152, 2013.
- [6] “Department of Health and Human Services: World’s older population grows dramatically,” <http://www.who.int/en/news-room/fact-sheets/detail/falls>, [Online; accessed 30-Oct-2018].
- [7] “World Healt Organization: Falls,” <http://www.who.int/en/news-room/fact-sheets/detail/falls>, [Online; accessed 30-Oct-2018].
- [8] S. S. Khan and J. Hoey, “Review of fall detection techniques: A data availability perspective,” *Medical engineering and physics*, vol. 39, pp. 12–22, 2017.
- [9] N. Lapierre, N. Neubauer, A. Miguel-Cruz, A. R. Rincon, L. Liu, and J. Rousseau, “The state of knowledge on technologies and their use for fall detection: A scoping review,” *International journal of medical informatics*, 2017.
- [10] N. Pannurat, S. Thiemjarus, and E. Nantajeewarawat, “Automatic fall monitoring: a review,” *Sensors*, vol. 14, no. 7, pp. 12900–12936, 2014.
- [11] T. Xu, Y. Zhou, and J. Zhu, “New advances and challenges of fall detection systems: A survey,” *Applied Sciences*, vol. 8, no. 3, pp. 418, 2018.

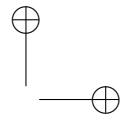
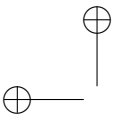
- [12] N. El-Bendary, Q. Tan, F. C. Pivot, and A. Lam, “Fall detection and prevention for the elderly: A review of trends and challenges.,” *International Journal on Smart Sensing & Intelligent Systems*, vol. 6, no. 3, 2013.
- [13] Q. Wu, Y. D. Zhang, W. Tao, and M. G. Amin, “Radar-based fall detection based on doppler time–frequency signatures for assisted living,” *IET Radar, Sonar & Navigation*, vol. 9, no. 2, pp. 164–172, 2015.
- [14] T. Liu, H. Yao, R. Ji, Y. Liu, X. Liu, X. Sun, P. Xu, and Z. Zhang, “Vision-based semi-supervised homecare with spatial constraint,” in *Pacific-Rim Conference on Multimedia*. Springer, 2008, pp. 416–425.
- [15] F. Werner, J. Diermaier, S. Schmid, and P. Panek, “Fall detection with distributed floor-mounted accelerometers: An overview of the development and evaluation of a fall detection system within the project ehome,” in *Pervasive Computing Technologies for Healthcare (PervasiveHealth), 2011 5th International Conference on*. IEEE, 2011, pp. 354–361.
- [16] Y. Zigel, D. Litvak, and I. Gannot, “A method for automatic fall detection of elderly people using floor vibrations and sound—proof of concept on human mimicking doll falls,” *IEEE Trans. Biomed. Eng.*, vol. 56, no. 12, pp. 2858–2867, 2009.
- [17] Y. Li, K. Ho, and M. Popescu, “A microphone array system for automatic fall detection,” *IEEE Trans. Biomed. Eng.*, vol. 59, no. 5, pp. 1291–1301, 2012.
- [18] M. Popescu, Y. Li, M. Skubic, and M. Rantz, “An acoustic fall detector system that uses sound height information to reduce the false alarm rate,” in *Engineering in Medicine and Biology Society, 2008. EMBS 2008. 30th Annual International Conference of the IEEE*. IEEE, 2008, pp. 4628–4631.
- [19] M. S. Khan, M. Yu, P. Feng, L. Wang, and J. Chambers, “An unsupervised acoustic fall detection system using source separation for sound interference suppression,” *Signal processing*, vol. 110, pp. 199–210, 2015.
- [20] X.-X. Zhang, H. Liu, Y. Gao, and D. H. Hu, “Detecting abnormal events via hierarchical dirichlet processes,” in *Pacific-Asia Conference on Knowledge Discovery and Data Mining*. Springer, 2009, pp. 278–289.
- [21] M. Popescu and A. Mahnot, “Acoustic fall detection using one-class classifiers,” in *Engineering in Medicine and Biology Society, 2009. EMBC 2009. Annual International Conference of the IEEE*. IEEE, 2009, pp. 3505–3508.

- [22] E. E. Stone and M. Skubic, “Fall detection in homes of older adults using the microsoft kinect,” *IEEE J. Biomed. Health Inform.*, vol. 19, no. 1, pp. 290–301, 2015.
- [23] A. Bourke, J. O’Brien, and G. Lyons, “Evaluation of a threshold-based tri-axial accelerometer fall detection algorithm,” *Gait and Posture*, vol. 26, no. 2, pp. 194–199, 2007.
- [24] Y. Charlon, N. Fourty, W. Bourennane, and E. Campo, “Design and evaluation of a device worn for fall detection and localization: Application for the continuous monitoring of risks incurred by dependents in an Alzheimer’s care unit,” *Expert Systems with Applications*, vol. 40, no. 18, pp. 7316–7330, 2013.
- [25] A. Özdemir and B. Barshan, “Detecting Falls with Wearable Sensors Using Machine Learning Techniques,” *Sensors*, vol. 14, no. 6, pp. 10691–10708, 2014.
- [26] M. Lustrek, H. Gjoreski, N. Gonzalez Vega, S. Kozina, B. Cvetkovic, V. Mirchevska, and M. Gams, “Fall detection using location sensors and accelerometers,” *Pervasive Computing*, vol. 14, no. 4, pp. 72–79, Oct 2015.
- [27] M. Alwan, P. J. Rajendran, S. Kell, D. Mack, S. Dalal, M. Wolfe, and R. Felder, “A smart and passive floor-vibration based fall detector for elderly,” in *Proc. of Inf. Commun. Technol.*, 2006, vol. 1, pp. 1003–1007.
- [28] A. Yazar, F. Keskin, B. U. Töreyin, and A. E. Çetin, “Fall detection using single-tree complex wavelet transform,” *Pattern Recognition Letters*, vol. 34, pp. 1945–1952, 2013.
- [29] X. Zhuang, J. Huang, G. Potamianos, and M. Hasegawa-Johnson, “Acoustic fall detection using Gaussian mixture models and GMM supervectors,” in *Proc. of ICASSP*, Taipei, Taiwan, Apr. 19-24 2009, pp. 69–72.
- [30] L. Liu, M. Popescu, M. Skubic, and M. Rantz, “An automatic fall detection framework using data fusion of Doppler radar and motion sensor network,” in *Proc. of the 36th International Conference of the Engineering in Medicine and Biology Society (EMBC)*, 2014, pp. 5940–5943.
- [31] C. N. Doukas and I. Maglogiannis, “Emergency fall incidents detection in assisted living environments utilizing motion, sound, and visual perceptual components,” *IEEE Trans. Inf. Technol. Biomed.*, vol. 15, no. 2, pp. 277–89, Mar. 2011.

- [32] B. Toreyin, A. Soyer, I. Onaran, and E. Cetin, “Falling person detection using multi-sensor signal processing,” *EURASIP Journal on Advances in Signal Processing*, vol. 2008, no. 1, pp. 7, 2008.
- [33] N. Noury, A. Fleury, P. Rumeau, A. Bourke, G. Laighin, V. Rialle, and J. Lundy, “Fall detection-principles and methods,” in *Engineering in Medicine and Biology Society, 2007. EMBS 2007. 29th Annual International Conference of the IEEE*. IEEE, 2007, pp. 1663–1666.
- [34] C. Cortes and V. Vapnik, “Support-vector networks,” *Machine learning*, vol. 20, no. 3, pp. 273–297, 1995.
- [35] C. Bishop, *Pattern Recognition and Machine Learning*, Springer Science+Business Media, LLC, New York, 2006.
- [36] B. Schölkopf, R. C. Williamson, A. J. Smola, J. Shawe-Taylor, and J. C. Platt, “Support vector method for novelty detection,” in *Advances in neural information processing systems*, 2000, pp. 582–588.
- [37] B. Schölkopf, R. C. Williamson, A. J. Smola, J. Shawe-Taylor, and J. C. Platt, “Support vector method for novelty detection,” in *Advances in Neural Information Processing Systems*. 2000, vol. 12, pp. 582–588, MIT Press.
- [38] S. Boyd and L. Vandenberghe, *Convex optimization*, Cambridge University Press, 2004.
- [39] D. E. Rumelhart, G. E. Hinton, and R. J. Williams, “Learning representations by back-propagating errors,” *Nature*, vol. 323, pp. 533–536, Oct. 1986.
- [40] Y. Lecun, L. Bottou, Y. Bengio, and P. Haffner, “Gradient-based learning applied to document recognition,” *Proceedings of the IEEE*, vol. 86, no. 11, pp. 2278–2324, Nov 1998.
- [41] I. Goodfellow, H. Lee, Q. V. Le, A. Saxe, and A. Y. Ng, “Measuring invariances in deep networks,” in *Advances in Neural Information Processing Systems 22*, Y. Bengio, D. Schuurmans, J. Lafferty, C. Williams, and A. Culotta, Eds., pp. 646–654. Curran Associates, Inc., 2009.
- [42] Y. Bengio, P. Lamblin, D. Popovici, and H. Larochelle, “Greedy layer-wise training of deep networks,” in *Advances in Neural Information Processing Systems 19*, B. Schölkopf, J. Platt, and T. Hoffman, Eds., pp. 153–160. MIT Press, 2007.
- [43] E. C. E. G. S. G. S. Spinsante, “Tst fall detection dataset v1,” 2016.

- [44] B. Kwolek and M. Kepski, “Human fall detection on embedded platform using depth maps and wireless accelerometer,” *Computer methods and programs in biomedicine*, vol. 117, no. 3, pp. 489–501, 2014.
- [45] I. Charfi, J. Miteran, J. Dubois, M. Atri, and R. Tourki, “Optimized spatio-temporal descriptors for real-time fall detection: comparison of support vector machine and adaboost-based classification,” *Journal of Electronic Imaging*, vol. 22, no. 4, pp. 041106, 2013.
- [46] A. T. Özdemir and B. Barshan, “Detecting falls with wearable sensors using machine learning techniques,” *Sensors*, vol. 14, no. 6, pp. 10691–10708, 2014.
- [47] E. Casilari, J.-A. Santoyo-Ramón, and J.-M. Cano-García, “Analysis of public datasets for wearable fall detection systems,” *Sensors*, vol. 17, no. 7, 2017.
- [48] M. Vacher, S. Bouakaz, M.-E. B. Chaumon, F. Aman, R. A. Khan, S. Bekkadja, F. Portet, E. Guillou, S. Rossato, and B. Lecouteux, “The cirdo corpus: Comprehensive audio/video database of domestic falls of elderly people,” in *Proceedings of the Tenth International Conference on Language Resources and Evaluation (LREC 2016)*, N. C. C. Chair), K. Choukri, T. Declerck, S. Goggi, M. Grobelnik, B. Maegaard, J. Marianni, H. Mazo, A. Moreno, J. Odijk, and S. Piperidis, Eds., Paris, France, may 2016, European Language Resources Association (ELRA).
- [49] P. Olivetti, “Sistema per la rilevazione e prevenzione di caduta anziani, mediante cassa di risonanza a pavimento,” Italian Patent 0001416548, July 1, 2015.
- [50] A. Temko, C. Nadeu, D. Macho, R. Malkin, and M. Omologo, “Acoustic Event Detection and Classification,” in *Hum. Comput. Interact. XXII, Comput. Hum. Interact. Loop*, W. Waibel and R. Stiefhagen, Eds., chapter 7, pp. 61–73. Springer-Verlag, Berlin, 2009.
- [51] T. Kinnunen and H. Li, “An overview of text-independent speaker recognition: From features to supervectors,” *Speech Communication*, vol. 52, no. 1, pp. 12–40, 2010.
- [52] J. A. Bilmes, “A gentle tutorial of the EM algorithm and its application to parameter estimation for Gaussian mixture and hidden Markov models,” Tech. Rep. ICSI-TR-97-021, University of Berkeley, 1997.
- [53] D. Reynolds and T. Quatieri, “Speaker verification using adapted gaussian mixture models,” *Digital Signal Process.*, vol. 10, no. 1, pp. 19–40, 2000.

- [54] C.-C. Chang and C.-J. Lin, “LIBSVM: a library for support vector machines,” *ACM Trans. Intell. Syst. Technol.*, vol. 2, no. 3, pp. 27, 2011.
- [55] C. Kim and R. M. Stern, “Power-normalized coefficients (PNCC) for robust speech recognition,” in *Proc. of ICASSP*, Kyoto, Japan, Mar. 2012, pp. 4101–4104.
- [56] S. B. Davis and P. Mermelstein, “Comparison of parametric representations for monosyllabic word recognition in continuously spoken sentences,” *IEEE Trans. Acoust., Speech, Signal Process.*, vol. 28, no. 4, pp. 357–366, 1980.
- [57] A. Temko and C. Nadeu, “Classification of acoustic events using SVM-based clustering schemes,” *Pattern Recognition*, vol. 39, no. 4, pp. 682–694, Apr. 2006.
- [58] A. Martin, G. Doddington, T. Kamm, M. Ordowski, and M. Przybocki, “The DET curve in assessment of detection task performance,” in *Proc. of the European Conference on Speech Communication and Technology*, 1997, pp. 1895–1898.
- [59] R. Rotili, S. Cifani, E. Principi, S. Squartini, and F. Piazza, “A robust iterative inverse filtering approach for speech dereverberation in presence of disturbances,” in *Proc. of IEEE Asia Pacific Conference on Circuits and Systems (APCCAS)*, Macao, China, Nov. 30 - Dec. 3 2008, pp. 434–437.
- [60] S. Cifani, E. Principi, C. Rocchi, S. Squartini, and F. Piazza, “A multichannel noise reduction front-end based on psychoacoustics for robust speech recognition in highly noisy environments,” in *Proc. of Hands-Free Speech Communication and Microphone Arrays (HSCMA)*, Trento, Italy, May 6-8 2008, pp. 172–175.
- [61] N. Noury, A. Fleury, P. Rumeau, A. Bourke, G. Laighin, V. Rialle, and J. Lundy, “Fall detection - principles and methods,” in *Proc. of the Annual Int. Conf. of the IEEE Engineering in Medicine and Biology Society (EMBC)*, Lyon, France, 2007, pp. 1663–1666.
- [62] M. Markou and S. Singh, “Novelty detection: a review – part 1: statistical approaches,” *Signal processing*, vol. 83, no. 12, pp. 2481–2497, 2003.
- [63] M. Markou and S. Singh, “Novelty detection: a review – part 2: neural network based approaches,” *Signal processing*, vol. 83, no. 12, pp. 2499–2521, 2003.
- [64] M. Popescu and A. Mahnot, “Acoustic fall detection using one-class classifiers,” in *Proc. of the Annual Int. Conf. of the IEEE Engineering in*



*Medicine and Biology Society (EMBC)*, Minneapolis, MN, USA, 2009, pp. 3505–3508.

- [65] E. Principi, S. Squartini, and F. Piazza, “Power Normalized Cepstral Coefficients based supervectors and i-vectors for small vocabulary speech recognition,” in *Proc. of the International Joint Conference on Neural Networks (IJCNN)*, Beijing, China, Jul. 6-11 2014, pp. 3562–3568.
- [66] U. Muller, J. Ben, E. Cosatto, B. Flepp, and Y. L. Cun, “Off-road obstacle avoidance through end-to-end learning,” in *Advances in neural information processing systems*, 2006, pp. 739–746.
- [67] J. Bergstra, D. Yamins, and D. Cox, “Making a science of model search: Hyperparameter optimization in hundreds of dimensions for vision architectures,” in *International Conference on Machine Learning*, 2013, pp. 115–123.
- [68] F. Werner, J. Diermaier, S. Schmid, and P. Panek, “Fall detection with distributed floor-mounted accelerometers: An overview of the development and evaluation of a fall detection system within the project eHome,” in *Proc. of the 5th Int. Conf. on Pervasive Computing Technologies for Healthcare and Workshops*, Dublin, Ireland, May 23-26 2011, pp. 354–361.
- [69] S. Dieleman and B. Schrauwen, “End-to-end learning for music audio,” in *Acoustics, Speech and Signal Processing (ICASSP), 2014 IEEE International Conference on*. IEEE, 2014, pp. 6964–6968.
- [70] A. Ng, “Sparse autoencoder,” *CS294A Lecture notes*, vol. 72, no. 2011, pp. 1–19, 2011.
- [71] A. Krizhevsky, I. Sutskever, and G. E. Hinton, “Imagenet classification with deep convolutional neural networks,” in *Advances in neural information processing systems*, 2012, pp. 1097–1105.
- [72] E. Marchi, F. Vesperini, S. Squartini, and B. Schuller, “Deep recurrent neural network-based autoencoders for acoustic novelty detection,” *Computational intelligence and neuroscience*, vol. 2017, 2017.
- [73] D. Kingma and J. Ba, “Adam: A method for stochastic optimization,” *arXiv preprint arXiv:1412.6980*, 2014.
- [74] X. Glorot and Y. Bengio, “Understanding the difficulty of training deep feedforward neural networks.,” in *Aistats*, 2010, vol. 9, pp. 249–256.

